Stable all-optical limiting in nonlinear periodic structures. II. Computations

Dmitry Pelinovsky

Department of Mathematics, McMaster University, Hamilton, Ontario, Canada L8S 4K1

Edward H. Sargent

Department of Electrical and Computer Engineering, University of Toronto, Toronto, Ontario, Canada M5S 1A4

Received September 28, 2001; revised manuscript received January 16, 2002

Transmission of coherent light through photonic gratings with varying Kerr nonlinearity is modeled within a coupled-mode system derived from the Maxwell equations. The incident light waves are uniformly stable in time-dependent dynamics if the photonic grating has zero net-average Kerr nonlinearity. When the average nonlinearity is weak but nonzero, light waves exhibit oscillatory instabilities and long-term high-amplitude oscillations in the out-of-phase linear gratings. We show that a two-step transmission map between lower-transmissive and higher-transmissive states has a narrow stability domain, which limits its applicability for logic and switching functions. Light waves exhibit cascades of real and complex instabilities in the multistable gratings with strong net-average Kerr nonlinearity. Only the first lower-transmissive stationary state can be stimulated by the incident light of small intensities. Light waves of moderate and large intensities are essentially nonstationary in the multistable gratings, and they exhibit periodic generation of Bragg solitons and blowup.

OCIS codes: 190.1450, 190.3100, 190.4360, 230.1480, 230.4320.

1. INTRODUCTION

Fiber-optic communications systems based on temporal solitons provide one promising avenue toward further increasing the bit rate and reach of the network infrastructure. Instead of being limited in their performance by dispersion and nonlinearity, such systems use the bandwidth and the intensity of ultrashort, coherent pulses emitted from mode-locked lasers to combine Kerr nonlinearity and chromatic dispersion to advantage, resulting in stable pulses propagating without intersymbol interference over ultralong-haul distances.

Ultimately, the goal of such systems is to reduce the extent to which signals must be amplified, reshaped, and retimed with expensive optical–electronic conversions. Instead, in-line processing of such pulses, purely within the optical domain and without undue demultiplexing and remultiplexing, would lead the way toward further reductions in the price per (bit $\times$ distance).

It is thus of interest to identify systematically how coherent ultrashort pulses will be processed by promising nonlinear elements. What will be the time response of the nonlinear devices? How would the intensity-dependent transmission characteristics be shaped and affect the pulse transmission?

In the present study, we answer these questions by studying transmission of coherent light of constant intensity through periodic nonlinear devices. This paper follows the recent publication[1] in which we considered the behavior of periodic materials consisting of alternating layers with different linear refractive indices and nonlinear Kerr coefficients.

Several physical parameters govern the transmission of optical signals through these nonlinear gratings. The condition for Bragg resonance between the light and the optical grating, the strength of periodic modulations of the refractive index, the net-average Kerr nonlinearity, and the variance of Kerr nonlinearities across different layers (nonlinearity management) determine optimal fabrication of photonic devices for signal-processing functions such as logic, limiting, and switching.[2] We showed from a steady-state analysis[1] that nonlinear periodic devices, given careful engineering of the nonlinear and linear components of the grating, can provide a stable, versatile basis for optical signal processing. Novel to the approach was a focus on reducing the net-average Kerr nonlinearity across the optical layers and in building an out-of-phase linear grating. It is these phenomena in combination that give rise to new and promising functions. However, it is essential to address the stability of these functions under the assumption of realistic fluctuations in physical parameters such as linear index and layer thickness. Such effects may give rise to temporal instabilities, noise generation, and other parasitics. We study the instability effects in the present, sequel paper. As our main result, we show that the useful optimal transmission map between lower-transmissive and higher-transmissive states has a narrow stability domain that limits its applicability for logic and switching functions.

2. MODEL AND STATIONARY-TRANSMISSION REGIMES

Signal processing in photonic gratings is based on matching the light frequency with the center of the bandgap in

photonic spectra. The photonic gratings exhibit the intensity-dependent response to the incident light that is modeled within the coupled-mode approximation of the Maxwell equations.[3]

The coupled-mode approximation is developed under several assumptions. First, the photonic grating is built up from extended layers of bulk optical materials. Second, the intensity of the incident wave and the variance of the refractive indices are considered to be small. Finally, the optical wavelength matches the first bandgap of the photonic spectrum (the Bragg resonance condition). Under these assumptions, the incident and reflected light in the optical material is modeled by the coupled-mode equations derived in Ref. 1:

$$i\left(\frac{\partial A_+}{\partial z} + \frac{\partial A_+}{\partial t}\right) + n_{0k}A_- + n_{nl}(|A_+|^2 + 2|A_-|^2)A_+ + n_{2k}[(2|A_+|^2 + |A_-|^2)A_- + A_+^2\bar{A}_-] = 0, \quad (1)$$

$$-i\left(\frac{\partial A_-}{\partial z} - \frac{\partial A_-}{\partial t}\right) + n_{0k}A_+ + n_{nl}(2|A_+|^2 + |A_-|^2)A_- + n_{2k}[(|A_+|^2 + 2|A_-|^2)A_+ + A_-^2\bar{A}_+] = 0, \quad (2)$$

where $A_+(z, t)$ and $A_-(z, t)$ are amplitudes of the incident and reflected waves, z and t are scaled space and time variables, and n_{0k}, n_{nl}, and n_{2k} are material parameters. The parameter n_{0k} represents the variance of the linear refractive index, i.e., the strength of the linear grating. The parameter n_{nl} stands for the average Kerr nonlinearity across the structure. The parameter n_{2k} is the variance of the Kerr nonlinearity between the layers, i.e., it measures the nonlinearity management of the grating. The positive sign $n_{2k} > 0$ is used henceforth for convenience.

We assume that the optical grating has a finite length L such that $z \in [0,L]$. The coherent light transmission through the photonic grating is stationary, when the amplitudes $A_\pm$ do not depend on time, i.e., when $A_\pm = A_\pm(z)$. The incident (I_{in}), reflected (I_{ref}), and transmitted (I_{out}) intensities are defined from stationary solutions of Eqs. (1) and (2) at the ends of the finite interval $z \in [0,L]$,

$$I_{in} = |A_+|^2(0), \quad I_{ref} = |A_-|^2(0), \quad I_{out} = |A_+|^2(L), \quad (3)$$

and the backward wave vanishes at the right end of the grating, $|A_-|^2(L) = 0$. We have used the backward finite-difference scheme (see Ref. 1) to find the time-independent solutions $A_\pm(z)$ of the system (1)–(2) starting from the boundary conditions at the right end $z = L$ and iterating back to the left end $z = 0$. Matching the values of $A_+(z)$ with the boundary conditions (3), we have analyzed the stationary transmission by plotting the transmitted intensity I_{out} versus the incident intensity I_{in}.

The stationary regimes are classified into three different types: (i) stable limiting, (ii) locally multistable limiting, and (iii) multistable regime. The three regimes are shown in Fig. 1 for the input–output transmission characteristic $I_{out} = I_{out}(I_{in})$. The corresponding optical grating has the material parameters $L = 20$, $n_{2k} = 1$, and different values of n_{nl} and n_{0k}.

The all-optical limiting regime is uniform for all pertinent incident intensities, i.e., the function $I_{out}(I_{in})$ is one-to-one (curves Ia and Ib in Fig. 1). The multistable regime shows up as branching of the function $I_{out}(I_{in})$ (curve III in Fig. 1), when several stationary transmissions may occur for the same value of the incident intensity I_{in}. The locally multistable limiting is an intermediate regime between all-optical limiting and multistability (curve II in Fig. 1). It exhibits branching for small and intermediate values of I_{in}, but it is clamped below the limiting value for I_{out} at large values of I_{in}. The existence domains I, II, and III of the three regimes are shown in Fig. 2 for the standardized photonic grating with $L = 20$ and $n_{2k} = 1$. The existence domains are derived from the coupled-mode system (1)–(2) (see Ref. 1 for details):

(i) The all-optical limiting regime occurs for optical gratings with strong nonlinearity management, when

$$n_{2k} \geqslant \frac{3}{4}|n_{nl}|. \quad (4)$$

If the nonlinearity is balanced exactly, i.e., $n_{nl} = 0$, the all-optical limiting occurs both for in-phase ($n_{0k} \geqslant 0$) and out-of-phase ($n_{0k} < 0$) optical gratings. However, the transmission characteristic $I_{out}(I_{in})$ then has two different shapes: it is concave downward for in-phase gratings (curve Ia in Fig. 1), but it is a two-step linear map for out-of-phase gratings (curve Ib in Fig. 1). This role of the out-of-phase gratings is explained by a threshold value $I_{out} = I_{thr} \equiv |n_{0k}|/n_{2k}$, when the varying part of the linear and Kerr nonlinear indices vanishes and the photonic grating becomes completely transparent (see Ref. 1). The Kerr nonlinearity management dominates over the

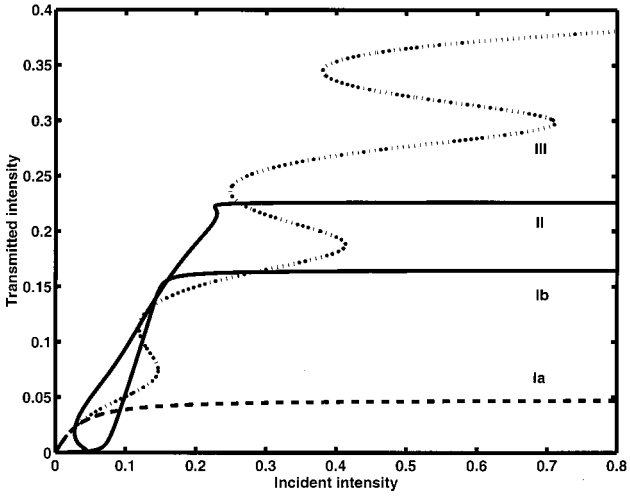

Fig. 1. Input–output transmission curve for the nonlinear periodic optical structure with parameters (Ia) $n_{nl} = 1$, $n_{0k} = 0$, (Ib) $n_{nl} = 0$, $n_{0k} = -0.15$, (II) $n_{nl} = 1$, $n_{0k} = -0.15$, and (III) $n_{nl} = 1.4$, $n_{0k} = 0$. The other material parameters are standardized as $L = 20$ and $n_{2k} = 1$. The photonic structure is in the stable all-optical limiting regime for curves Ia and Ib, the locally multistable limiting regime for curve II, and the multistable regime for curve III.

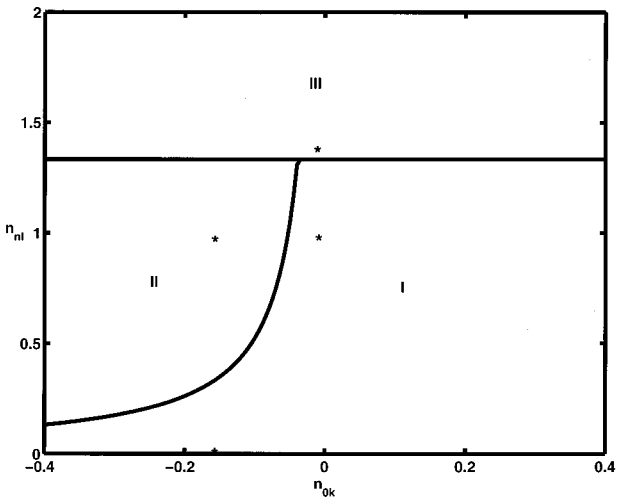

Fig. 2. Existence domains I, II, and III of the three stationary regimes of photonic gratings: (i) stable all-optical limiting, (ii) locally multistable limiting, and (iii) multistability on the plane (n_{0k}, n_{nl}). The other material parameters are standardized as $L = 20$ and $n_{2k} = 1$. The particular parameter values from Fig. 1 are marked by stars.

linear grating for $I_{out} > I_{thr}$, but it is smaller than the linear grating for $I_{out} < I_{thr}$. If the balance of Kerr nonlinearities is broken, i.e., $n_{nl} \neq 0$, the all-optical limiting is preserved only for in-phase or weak out-of-phase gratings under the constraint

$$n_{0k} \geq -\frac{\pi n_{2k}}{3|n_{nl}|L}. \tag{5}$$

The latter condition detects the threshold when the stationary distribution $I_{\pm} = |A_{\pm}|^2(z)$ becomes nonmonotonic in z. We notice that this condition is not directly related to the threshold when the curve $I_{out}(I_{in})$ becomes multivalued. However, these two thresholds are close to each other. The domain for the all-optical limiting regime is shown in Fig. 2 as domain I.

(ii) When the constraint (4) is held but the constraint (5) is violated, i.e., for strong out-of-phase gratings with $n_{0k} < 0$, the light transmission has local multistability for the intermediate range of incident intensities and final limiting at large values of I_{in} (curve II in Fig. 1). The local multistability occurs due to the dominant role of the linear grating for subthreshold values of $I_{out} < I_{thr}$. It follows from constraint (5) that it is hard to maintain the two-step linear map as in curve Ib of Fig. 1. Longer structures or weaker nonlinearity management lead to local branching and multistability of the out-of-phase grating with $n_{nl} \neq 0$. The domain for the locally multistable limiting regime is shown in Fig. 2 as domain II.

(iii) When the constraint (4) is violated, i.e., for optical gratings under weak nonlinearity management and strong net-average nonlinearity, the light transmission is multistable for all ranges of incident intensities (curve III in Fig. 1). When the nonlinearity management is negligible, i.e., when $n_{2k} = 0$, the input–output transmission curve $I_{out}(I_{in})$ has the S-bistable shape that is well known in the approximation of an average Kerr nonlinearity (see review in Ref. 3). The multistability domain is shown in Fig. 2 as domain III.

The three regimes above were classified by use of the bistability theory known in the physics of periodic structures.[4–7] It is usually believed[3] that the stationary light transmission with the output intensity corresponding to a negative slope of the curve $I_{out} = I_{out}(I_{in})$ is linearly unstable. The hypothesis was confirmed numerically by de Sterke,[8] who identified real unstable eigenvalues of the linear stability problem associated with the negative-slope stationary transmission. De Sterke considered the coupled-mode system (1)–(2) in the case $n_{2k} = 0$ (no nonlinearity management).

A different analytical method was developed recently by Ovchinnikov[9] who confirmed instability of the negative-slope stationary transmission. Ovchinnikov considered the one-dimensional Maxwell equation describing a layer of uniform nonlinear optical material. In this case, i.e., for $n_{0k} = n_{2k} = 0$, the coupled-mode system (1)–(2) has no stationary solutions satisfying the boundary conditions (3). Therefore the stationary-transmission regimes considered in Ref. 9 are beyond the coupled-mode approximation.

The linear stability results are unknown for the coupled-mode system (1)–(2) in a general case. First, no mathematical theory exists to date, to our knowledge, to confirm the instability and bifurcations for the negative-slope light transmission. Second, even for the most studied cases, a complicated instability pattern was observed,[8,9] when not only negative-slope transmissive states but also positive-slope highly transmissive states were linearly unstable due to complex eigenvalues of the linear stability problem. The large-amplitude pulsations result from instability of highly transmissive states, and these pulsations may lead to chaotic dynamics of light in the photonic grating.[10,11]

We proved analytically in Ref. 1 that the all-optical limiting regime is linearly stable in optical gratings with balanced nonlinearity management (when $n_{nl} = 0$). No real or complex eigenvalues of the linear stability problem may exist in this case. Thus we concluded that any nonstationary dynamics of the nonlinearity-compensated optical grating is expected to converge to the stationary light transmission for a given value of the incident intensity I_{in}. However, this stability result is very special since it is based on integrability of the linear stability problem for $n_{nl} = 0$.

In this paper we study numerically the linear stability and the nonstationary dynamics of photonic gratings, when the nonlinearity is not compensated exactly, i.e., when $n_{nl} \neq 0$. We deploy an original numerical method based on finite differences and use it to quantify the nonstationary light transmission through photonic gratings. We show that the in-phase gratings ($n_{0k} \geq 0$) remain stable for $n_{nl} \neq 0$ in the domain I (see Fig. 2). In this case, the all-optical limiting transmission curve $I_{out}(I_{in})$ is concave downward as in curve Ia of Fig. 1. However, the out-of-phase gratings ($n_{0k} < 0$) are destabilized at $n_{nl} \neq 0$ due to oscillatory instabilities arising for larger negative n_{0k}. Thus the all-optical limiting regime with the two-step linear map as in curve Ib of Fig. 1, while stable for $n_{nl} = 0$, exhibits instabilities for weaker nonlinearity management, when $n_{nl} \neq 0$. Furthermore, we show that there exist several real and complex unstable

eigenvalues of the linear stability problem in the domains II and III (see Fig. 2). These instabilities and the nonstationary dynamics of exponentially growing perturbations generalize the results of de Sterke[8] for photonic gratings with no nonlinearity management ($n_{2k} = 0$).

There are several methods developed for numerical modeling of the coupled-mode system (1)–(2) for $n_{2k} = 0$. The split-step spectral method is widely used in nonlinear optics for numerical modeling of time-evolution problems.[12] The split-step method is second order in time, and it is usually time consuming compared with finite-difference methods. An alternative collocation method based on an implicit Runge–Kutta method is developed for the couple-mode system by de Sterke *et al.*[13] The collocation method is fourth order in time, but it is substantially faster than spectral methods. Although the collocation method is well suited to solve the time-evolution problem associated with the system (1)–(2), it has some limitations. The collocation method uses the coordinate transformations to rotate the system (1)–(2) along to the wave characteristics $z \pm t$. As a result, the time step size cannot be different from the space step size. Also the method cannot be extended to solving the linear stability problem and computing unstable eigenvalues for stationary-transmission regimes.

In the present paper, we use the Crank–Nicholson implicit method based on second-order finite differences in order to compute both the time-evolution problem and the linear eigenvalue problem associated with the coupled system (1)–(2). A complete software package enables us to solve several computational problems for dynamics of photonic gratings: (i) to obtain the stationary regime, (ii) to compute stable and unstable eigenvalues of the stationary regime in the linear stability problem, (iii) to simulate perturbations of the stationary regime in the time-evolution problem, and (iv) to model nonstationary transmission under a variable intensity of the incident light.

The computational results are described in the paper in the following order. Section 3 presents the finite-difference method applied to the coupled system (1)–(2). Several characteristic time evolutions associated with stable limiting, locally multistable limiting, and multistable transmission regimes are described in Section 4. Unstable eigenvalues are computed in Section 5, where stability analysis of stationary regimes is quantified. Transitions to stationary or nonstationary regimes stimulated by the incident light are modeled in Section 6. The different possibilities are matched with existence of unstable eigenvalues in the linear stability problem. Details of the numerical methods for Sections 3 and 5 are given in Appendixes A and B.

3. NUMERICAL METHOD

When the periodic optical material is illuminated by the incident light, the coupled-mode system (1)–(2) is modeled at the finite interval $z \in [0,L]$ subject to the boundary conditions

$$A_+(0,t) = \sqrt{I_{\text{in}}}\exp(i\theta_{\text{in}}), \quad A_-(L,t) = 0, \tag{6}$$

where $I_{\text{in}} = I_{\text{in}}(t)$ and $\theta_{\text{in}} = \theta_{\text{in}}(t)$ represent the amplitude and phase modulations of the incident light. The complex-valued system (1)–(2) can be decomposed into the real and imaginary parts

$$A_+ = u + iw, \quad A_- = v + iy. \tag{7}$$

The real functions u, w, v, and y satisfy the coupled system

$$\frac{\partial u}{\partial t} + \frac{\partial u}{\partial z} + n_{0k}y + f_u = 0,$$

$$-\frac{\partial y}{\partial t} + \frac{\partial y}{\partial z} + n_{0k}u + f_y = 0, \tag{8}$$

$$-\frac{\partial w}{\partial t} - \frac{\partial w}{\partial z} + n_{0k}v + f_w = 0,$$

$$\frac{\partial v}{\partial t} - \frac{\partial v}{\partial z} + n_{0k}w + f_v = 0, \tag{9}$$

where the nonlinear (cubic) functions are given by

$$f_u = f(u,w,v,y), \quad f_w = f(w,u,y,v),$$

$$f_v = f(v,y,u,w), \quad f_y = f(y,v,w,u), \tag{10}$$

$$f(u,w,v,y) = n_{\text{nl}}(u^2 + w^2 + 2v^2 + 2y^2)w + n_{2k}[(u^2 + 3w^2 + v^2 + y^2)y + 2uwv]. \tag{11}$$

In neglection of the nonlinear function $f(u,w,v,y)$, the system (8)–(9) can be further decomposed into two partial subsystems for (u,y) and (w,v). Each subsystem reduces to a scalar wave (Klein–Gordon) equation, e.g., for the function $u = u(z,t)$:

$$\frac{\partial^2 u}{\partial t^2} - \frac{\partial^2 u}{\partial z^2} + n_{0k}^2 u = 0. \tag{12}$$

In the finite-difference method, the functions u, w, v, and y are approximated on the grid

$$z = z_n = nh, \quad n = 0,1,\ldots,N, \ (N+1), \tag{13}$$

where h is the space step size, and the grid has N interior points and two end points at $z_0 = 0$ and $z_{N+1} = (N+1)h = L$, i.e., $h = L/(N+1)$. For time evolution, the functions u, w, v, and y are defined at the time instances $t = t_k = k\tau$, where $k = 0,1,\ldots,K$, and τ is the time step size. For each time instance $t = t_k$, we introduce the vectors of unknowns

$$\mathbf{u}_k = \begin{bmatrix} u_{1,k} \\ u_{2,k} \\ \cdot \\ \cdot \\ \cdot \\ u_{N,k} \\ u_{N+1,k} \end{bmatrix}, \quad \mathbf{w}_k = \begin{bmatrix} w_{1,k} \\ w_{2,k} \\ \cdot \\ \cdot \\ \cdot \\ w_{N,k} \\ w_{N+1,k} \end{bmatrix},$$

$$\mathbf{v}_k = \begin{bmatrix} v_{0,k} \\ v_{1,k} \\ \cdot \\ \cdot \\ \cdot \\ v_{N-1,k} \\ v_{N,k} \end{bmatrix}, \quad \mathbf{y}_k = \begin{bmatrix} y_{0,k} \\ y_{1,k} \\ \cdot \\ \cdot \\ \cdot \\ y_{N-1,k} \\ y_{N,k} \end{bmatrix}. \tag{14}$$

The values $u_{N+1,k}$, $w_{N+1,k}$ and $v_{0,k}$, $y_{0,k}$ are boundary values at the end points $z = L$ and $z = 0$, respectively. These values are also unknown at each time instance in contrast to the boundary values $u_{0,k}$, $w_{0,k}$ and $v_{N+1,k}$, $y_{N+1,k}$ that follow from the boundary conditions (6) as

$$\begin{aligned} u_{0,k} &= \sqrt{I_{\text{in}}(t_k)} \cos \theta_{\text{in}}(t_k), \\ w_{0,k} &= \sqrt{I_{\text{in}(t_k)}} \sin \theta_{\text{in}}(t_k), \\ v_{N+1,k} &= 0, \quad y_{N+1,k} = 0. \end{aligned} \tag{15}$$

The scalar wave equation (12) is numerically modeled by the implicit Crank–Nicholson method:

$$\begin{aligned} &\frac{u_{n,k+1} - 2u_{n,k} + u_{n,k-1}}{\tau^2} + \frac{n_{0\text{k}}^2 (u_{n,k+1} + u_{n,k-1})}{2} \\ &\quad - \frac{u_{n+1,k+1} - 2u_{n,k+1} + u_{n-1,k+1}}{2h^2} \\ &\quad - \frac{u_{n+1,k-1} - 2u_{n,k-1} + u_{n-1,k-1}}{2h^2} = 0. \end{aligned} \tag{16}$$

The numerical method (16) is known to be unconditionally stable for any values of τ, h, and $n_{0\text{k}}$. The global truncation error of the finite (central) difference approximations for partial derivatives has the order of $O(\tau^2 + h^2)$. The details of the numerical method for the complete system (8)–(9) are described in Appendix A. Given the starting values at $k = 0$ and $k = 1$ for the vectors in Eqs. (14), the time steps are performed by solving the following linear systems for $k \geq 1$,

$$\begin{bmatrix} A(r) & \kappa I_+ \\ -\kappa I_- & B(r) \end{bmatrix} \begin{bmatrix} \mathbf{u}_{k+1} \\ \mathbf{y}_{k+1} \end{bmatrix} = \begin{bmatrix} A(-r) & -\kappa I_+ \\ \kappa I_- & B(-r) \end{bmatrix} \begin{bmatrix} \mathbf{u}_{k-1} \\ \mathbf{y}_{k-1} \end{bmatrix} + \begin{bmatrix} \mathbf{H}_{u\ k} \\ \mathbf{H}_{y\ k} \end{bmatrix}, \tag{17}$$

$$\begin{bmatrix} A(r) & -\kappa I_+ \\ \kappa I_- & B(r) \end{bmatrix} \begin{bmatrix} \mathbf{w}_{k+1} \\ \mathbf{v}_{k+1} \end{bmatrix} = \begin{bmatrix} A(-r) & \kappa I_+ \\ -\kappa I_- & B(-r) \end{bmatrix} \begin{bmatrix} \mathbf{w}_{k-1} \\ \mathbf{v}_{k-1} \end{bmatrix} + \begin{bmatrix} \mathbf{H}_{w\ k} \\ \mathbf{H}_{v\ k} \end{bmatrix}, \tag{18}$$

where

$$r = \frac{\tau}{2h}, \quad \kappa = \tau n_{0\text{k}}, \tag{19}$$

while the matrices $A(r)$, $B(r)$, I_+, and I_- and the nonlinear functions $\mathbf{H}_u$, $\mathbf{H}_w$, $\mathbf{H}_v$, and $\mathbf{H}_y$ are all given in Eqs. (A9)–(A15) of Appendix A. Since initial conditions define only the first starting approximation for the vectors $\mathbf{u}_0$, $\mathbf{w}_0$, $\mathbf{v}_0$, and $\mathbf{y}_0$, the first time step is to be performed separately. An explicit two-point predictor–corrector method is used to approximate the vectors $\mathbf{u}_1$, $\mathbf{w}_1$, $\mathbf{v}_1$, and $\mathbf{y}_1$.

In the numerical computations described in the paper, we have standardized the periodic optical grating at the fixed length $L = 20$ with $N = 200$ grid points. The variance of the Kerr nonlinearity is standardized as $n_{2\text{k}} = 1$ without loss of generality. The time step τ is chosen to reduce the nonlinear effects produced by the vectors $\mathbf{H}_u$, $\mathbf{H}_w$, $\mathbf{H}_v$, and $\mathbf{H}_y$ in Eqs. (17)–(18). Indeed, the linearly stable numerical method can be destabilized by large nonlinearities. We define the time step τ in the form

$$\tau = \begin{cases} 0.5h & hM < 0.002 \\ 0.001M^{-1} & hM > 0.002' \end{cases} \tag{20}$$

where $M = \max_{0 \leq t \leq T} [I_{\text{in}}(t)]^{3/2}$. If the nonlinear functions $\mathbf{H}_u$, $\mathbf{H}_w$, $\mathbf{H}_v$, and $\mathbf{H}_y$ are smaller than order of $O(10^{-3})$, the time step size is matched with the space step size: $\tau = 0.5h$. Otherwise, the nonlinear functions are reduced to the order of $O(10^{-3})$ by reducing the time step size τ according to the second line in Eq. (20).

4. TIME-DEPENDENT DYNAMICS OF NEAR-STATIONARY LIGHT TRANSMISSION

Here we test the numerical method and model the time-dependent dynamics of near-stationary light waves. First, we consider the grating under balanced nonlinearity management, when $n_{\text{nl}} = 0$. In the latter case, the stationary regimes $A_\pm = A_{\pm 0}(z)$ were proven analytically to be linearly stable.[1] To confirm this fact, we set the initial condition in the form of a perturbed stationary distribution:

$$\begin{aligned} A_+(z, 0) &= A_{+0}(z), \\ A_-(z, 0) &= A_{-0}(z)[1 + \alpha \exp(-z)], \end{aligned} \tag{21}$$

where α is the perturbation factor and the exponential function localizes the perturbation near the left boundary at $(\Delta z) \approx 1 \ll L = 20$, where the incident wave is illuminated. The dynamics of the light transmission in the case $n_{\text{nl}} = 0$ is very simple even for moderate perturbation, $\alpha = 0.1$. The perturbation disappears due to emission of the reflected and transmitted radiations through the ends of the optical material. As a result, the transient dynamics induced by the perturbation quickly converges to the stationary regime $A_\pm = A_{\pm 0}(z)$. We have checked that this possibility is observed both for in-phase ($n_{0\text{k}} \geq 0$) and out-of-phase ($n_{0\text{k}} < 0$) linear gratings, when the net-average Kerr nonlinearity is compensated exactly, i.e., $n_{\text{nl}} = 0$. This numerical result confirms conclusions of Ref. 1.

Now we turn to the in-phase linear grating when the Kerr nonlinearity is not compensated, i.e., when $n_{\text{nl}} \neq 0$ and $n_{0\text{k}} \geq 0$. Under the constraint (4), the in-phase photonic gratings are in the all-optical limiting regime across the layers, and they have a one-to-one concave downward transmission curve $I_{\text{out}}(I_{\text{in}})$, as in curve Ia of Fig. 1 for $n_{0\text{k}} = 0$ and $n_{\text{nl}} = 1$. The numerical evolution of the perturbed stationary distribution (21) is shown in Fig. 3 for $\alpha = 0.1$ and $I_{\text{out}} = 0.04$. The perturbation factor induces a wave packet in the forward wave A_+ that propagates all

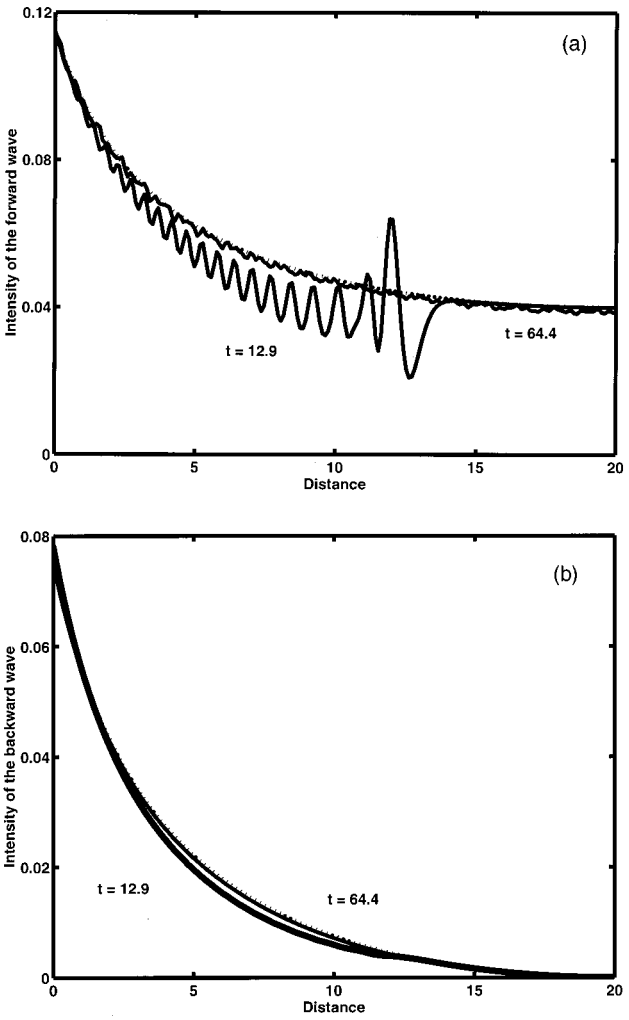

Fig. 3. Intensities of (a) the forward and (b) backward waves in different time instances: $t = 12.9$ and $t = 64.4$. The stationary distribution is shown by a dotted curve for $I_{out} = 0.04$. The standardized photonic structure has the material parameters $n_{nl} = 1$ and $n_{0k} = 0$ (see curve Ia in Fig. 1). The perturbation of the stationary transmission disappears by means of radiation through the ends of the structure.

the way from the left to the right end of the structure and radiates away [see Fig. 3(a)]. The backward wave A_- remains smooth during transmission of the wave packet and follows this process with small distortion [see Fig. 3(b)]. After the packet is radiated away, the light transmission settles at a stable stationary regime with $I_{out} = 0.04$ (dotted curves in Fig. 3). A relatively large transient radiation is the only difference of the dynamics of in-phase photonic grating for $n_{nl} \neq 0$ compared with that for $n_{nl} = 0$.

A different possibility is observed for the out-of-phase linear gratings when the Kerr nonlinearity is not compensated, i.e., when $n_{nl} \neq 0$ and $n_{0k} < 0$. When the constraint (5) is violated but the constraint (4) is preserved, the stationary limiting regime becomes locally multistable for small and intermediate values of I_{in}, as in curve II of Fig. 1 for $n_{0k} = -0.15$ and $n_{nl} = 1$. The local multistability occurs from a deformation of the two-step linear map $I_{out}(I_{in})$ that is uniformly stable for $n_{nl} = 0$ (compare curves Ib and II in Fig. 1). The local multistability of the out-of-phase photonic gratings exhibits the much more complicated dynamics shown in Fig. 4. A small initial perturbation of the stationary distribution

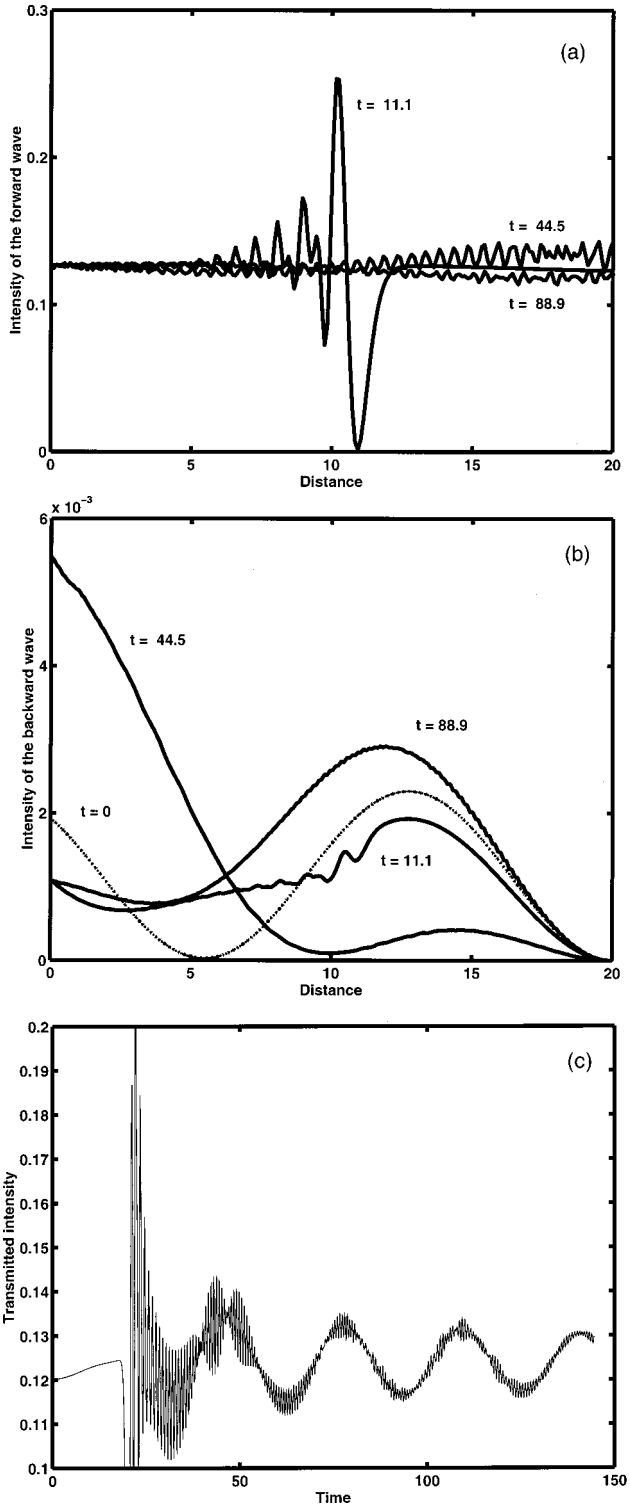

Fig. 4. Intensities of (a) the forward and (b) backward waves in different time instances: $t = 11.1$, $t = 44.5$, and $t = 88.9$. The initial (almost stationary) distribution at $t = 0$ is shown by a dotted curve for $I_{out} = 0.12$. The standardized photonic structure has the material parameters $n_{nl} = 1$ and $n_{0k} = -0.15$ (see curve II in Fig. 1). The stationary regime is unstable, and the light transmission exhibits high-amplitude oscillations. The transmitted intensity I_{out} as a function of time t is shown in (c).

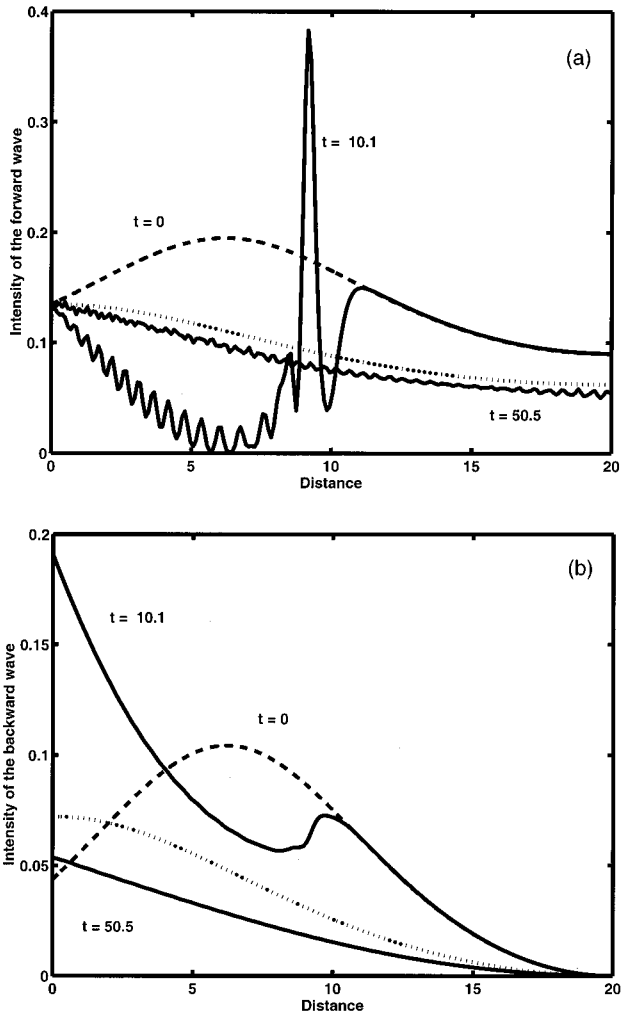

Fig. 5. Intensities of (a) the forward and (b) backward waves in different time instances: $t = 10.1$ and $t = 50.5$. The initial unstable stationary regime at $t = 0$ is shown by a dashed curve for $I_{out} = 0.09$. The final stable stationary regime is shown by a dotted curve for $I_{out} = 0.062$. Both the regimes are stimulated by the same incident intensity, $I_{in} = 0.135$. The standardized photonic structure has the material parameters $n_{nl} = 1.4$ and $n_{0k} = 0$ (see curve III in Fig. 1). The time-dependent dynamics of the periodic structure results in switching from an unstable highly transmissive state to a stable lower-transmissive state.

(21) with $\alpha = 0.01$ and $I_{out} = 0.12$ induces a large-amplitude wave packet transmitted from the left to the right end of the structure [see Fig. 4(a)]. Contrary to the stable dynamics shown in Fig. 3, the light transmission in the unstable out-of-phase grating does not become stationary after the wave packet passes away. Instead, periodic oscillations are induced in the structure [see Fig. 4(b)]. The oscillations have large amplitude but still resemble the unstable stationary distribution [shown by the dotted curve in Fig. 4(b)]. The oscillations are clearly seen in Fig. 4(c), where we plot the transmitted intensity $I_{out} = |A_+|^2(L, t)$ as a function of time t.

When the Kerr nonlinearity management is weak and the constraint (4) is violated, the stationary transmission becomes multistable, as in curve III of Fig. 1 for $n_{0k} = 0$ and $n_{nl} = 1.4$. The negative-slope transmission regimes are known to switch to positive-slope lower-intensity transmissive states or to large-amplitude oscillations near higher-intensity transmissive states.[3] Figure 5 illustrates the switching of the unstable stationary regime at $I_{out} = 0.09$ (dashed curve) under the perturbation (21) with $\alpha = 0.01$ to a stable lower-transmissive stationary regime at $I_{out} = 0.062$ (dotted curve). The value of the incident intensity I_{in} is the same for both the regimes: $I_{in} = 0.135$. The switching occurs through a transition front wave that moves across the structure from the left to the right ends [see Fig. 5(a)]. Relaxation rather than oscillatory dynamics is observed in the switching transition [see Fig. 5(b)].

Thus we summarize that there are three general types of dynamics of light waves transmitted in nonlinear periodic structures: (i) relaxation to a stable stationary state, (ii) oscillations near an unstable stationary state, and (iii) switching from unstable to stable stationary states. We explain the three characteristic time-evolution patterns by studying the unstable eigenvalues of the linear stability problem associated with a stationary-transmission regime.

5. LINEAR STABILITY AND UNSTABLE EIGENVALUES

Here we compute the spectrum of stable and unstable eigenvalues associated with a stationary-transmission regime in the coupled-mode system (1)–(2). The stationary regime corresponds to the time-independent solution $A_\pm = A_{\pm 0}(z)$ that satisfies the boundary conditions (3). We consider a small perturbation to the time-independent solution, separate the real and imaginary parts according to Eqs. (7), and define the time evolution constant λ in the form

$$u = u_0(z) + u_1(z)\exp(\lambda t),$$

$$w = w_0(z) + w_1(z)\exp(\lambda t), \tag{22}$$

$$v = v_0(z) + v_1(z)\exp(\lambda t),$$

$$y = y_0(z) + y_1(z)\exp(\lambda t). \tag{23}$$

We assume that the wave emission outside the periodic structure is not affected by the perturbation, i.e., the incident wave has the same input values I_{in} and θ_{in} as in the stationary regime [see Eqs. (6)]. Therefore the perturbation terms in Eqs. (22)–(23) satisfy the zero boundary conditions:

$$u_1(0) = w_1(0) = v_1(L) = y_1(L) = 0. \tag{24}$$

The time-evolution constant λ defines the spectrum of the stationary regime. If $\mathrm{Re}(\lambda) > 0$, the spectrum is unstable, i.e., a small perturbation $(u_1, w_1, v_1, y_1)(z)$ satisfying the zero boundary conditions (24) grows exponentially in time and destroys eventually the stationary transmission through the periodic optical structure. The perturbation terms satisfy a linear eigenvalue problem

with the Dirac-type complex operator (see Ref. 1). Separating the real and imaginary parts, the linear eigenvalue problem can be written as

$$-\frac{\partial u_1}{\partial z} - n_{0k} y_1 - f'_u = \lambda u_1, \quad \frac{\partial y_1}{\partial z} + n_{0k} u_1 + f'_y = \lambda y_1, \tag{25}$$

$$-\frac{\partial w_1}{\partial z} + n_{0k} v_1 + f'_w = \lambda w_1, \quad \frac{\partial v_1}{\partial z} - n_{0k} w_1 - f'_v = \lambda v_1, \tag{26}$$

where the linearized functions f'_u, f'_w, f'_v, and f'_y are constructed from a function $f'(u, w, v, y)$ according to the same rule as in Eq. (10). The function $f'(u, w, v, y)$ is the Frechet derivative of $f(u, w, v, y)$ at the stationary solution (u_0, w_0, v_0, y_0) with the perturbation (u_1, w_1, v_1, y_1):

$$\begin{aligned} f' = n_{nl}[&2u_0 w_0 u_1 + (u_0^2 + 3w_0^2 + 2v_0^2 + 2y_0^2) w_1 \\ &+ 4w_0 v_0 v_1 + 4w_0 y_0 y_1] \\ &+ n_{2k}[2(u_0 y_0 + w_0 v_0) u_1 + 2(3w_0 y_0 + u_0 v_0) w_1 \\ &+ 2(u_0 w_0 + v_0 y_0) v_1 + (u_0^2 + 3w_0^2 + v_0^2 + y_0^2) y_1]. \end{aligned} \tag{27}$$

Appendix B describes the finite-difference method applied to the linear eigenvalue problem (25)–(26). The unknown functions u_1, w_1, v_1, and y_1 are discretized on the grid (13). They can be grouped into the vectors of unknowns given in Eqs. (14). Dropping the subindex for the vectors **u**, **w**, **v**, and **y**, we reduce the linear eigenvalue problem (25)–(26) to the matrix eigenvalue problem:

$$\begin{bmatrix} A_\infty & -\kappa I_+ & 0 & 0 \\ \kappa I_- & B_\infty & 0 & 0 \\ 0 & 0 & A_\infty & \kappa I_+ \\ 0 & 0 & -\kappa I_- & B_\infty \end{bmatrix} \begin{bmatrix} \mathbf{u} \\ \mathbf{y} \\ \mathbf{w} \\ \mathbf{v} \end{bmatrix} + \mathcal{U} \begin{bmatrix} \mathbf{u} \\ \mathbf{y} \\ \mathbf{w} \\ \mathbf{v} \end{bmatrix} = \gamma \begin{bmatrix} \mathbf{u} \\ \mathbf{y} \\ \mathbf{w} \\ \mathbf{v} \end{bmatrix}, \tag{28}$$

where

$$\kappa = 2h n_{0k}, \quad \gamma = 2h\lambda, \tag{29}$$

the matrices $I_\pm$ are defined in Eqs. (A11) of Appendix A, and the matrices A_∞, B_∞, and $\mathcal{U}$ are given in Eqs. (B9)–(B11) of Appendix B.

The standard MATLAB computational package of numerical linear algebra can be used to find the spectrum of the matrix eigenvalue problem (28). The advantage of this approach is that the whole spectrum of stable and unstable eigenvalues is deduced from a single computation of the problem (28). The numerical error for the eigenvalues λ is of the order of $O(h^2)$, as it follows from the truncation error of the second-order finite differences.

Below, we report the principal results on the existence of unstable eigenvalues in the linear eigenvalue problem (25)–(26). First, we consider a simple case $I_{out} = 0$, when the problem can be studied analytically since $u_0 = w_0 = v_0 = y_0 = 0$ and $f' = 0$. The linear systems (25) and (26) are uncoupled, and the spectrum of eigenvalues is double degenerate. Each uncoupled subsystem can be solved exactly, e.g.,

$$u_1 = n_{0k} \sin kz, \quad y_1 = -\lambda \sin kz - k \cos kz, \tag{30}$$

where $\lambda^2 + n_{0k}^2 + k^2 = 0$. It follows from the boundary conditions $u_1(0) = y_1(L) = 0$ that $\lambda = -k \cot(kL)$. As a result, the parameter k satisfies the algebraic equation

$$1 + n_{0k}^2 \frac{\sin^2(kL)}{k^2} = 0. \tag{31}$$

Solutions of this equation do not exist for real values of k and λ. However, there are solutions for complex values of k and λ. We show the double-degenerate branch of the spectrum of λ in Fig. 6(a) as it is found from Eq. (31). The spectrum of λ is located in the asymptotically stable domain, where $\mathrm{Re}(\lambda) < 0$. The two largest eigenvalues are closest to the origin $\lambda = 0$: they have $\mathrm{Re}(\lambda) \approx -0.0311$ and $\mathrm{Im}(\lambda) \approx \pm 0.2074$. Notice that complex eigenvalues are symmetric with respect to the axis: $\mathrm{Im}(\lambda) = 0$. Indeed, since the linear eigenvalue problem (25)–(26) has real coefficients, it has either real or complex-conjugate eigenvalues. In order to test the finite-difference approximation used to replace the system (25)–(26) by the matrix eigenvalue problem (28), we construct analytical solutions to Eqs. (B1)–(B4) of Appendix B in the case $I_{out} = 0$. The system (B1)–(B4) is decoupled for $F' = 0$, and the discrete analogue of Eq. (30) is

$$\begin{aligned} u_1 &= n_{0k} \sin(knh), \\ y_1 &= -\lambda \sin(knh) - \frac{\sin(kh)}{h} \cos knh, \end{aligned} \tag{32}$$

where $\lambda^2 + n_{0k}^2 + \sin^2(kh)/h^2 = 0$. The boundary conditions $u_0 = y_{N+1} = 0$ are satisfied with $\lambda = -\sin(kh)\cot(kL)/h$, such that the parameter k satisfies the algebraic equation

$$1 + (n_{0k} h)^2 \frac{\sin^2(kL)}{\sin^2(kh)} = 0. \tag{33}$$

The spectrum of λ is shown in Fig. 6(b) as it is found from Eq. (33). The two branches are still located in the stable left half-plane of λ, but they move toward the axis $\mathrm{Re}(\lambda) = 0$ for larger values of $\mathrm{Im}(\lambda)$. This is the artifact following from truncation of continuous derivatives by their central-difference approximations. However, the spectrum is not affected near the origin, with the two largest eigenvalues being at $\mathrm{Re}(\lambda) \approx -0.0311$ and $\mathrm{Im}(\lambda) \approx \pm 0.2074$.

The matrix eigenvalue problem (28) is derived when the system (B1)–(B4) is modified by the end-point equations (B5)–(B8) in Appendix B. This modification deforms the spectrum of λ. The double branches of the spectrum are shown in Fig. 6(c) as it is found from Eq. (28) for $I_{out} = 0$. However, the deformation of the spectrum occurs for larger values of $\mathrm{Im}(\lambda)$, such that the eigenvalues closest to the origin of λ are computed with the same accuracy: $\mathrm{Re}(\lambda) \approx -0.0311$ and $\mathrm{Im}(\lambda) \approx \pm 0.2074$.

Thus the numerical results are expected to be accurate for eigenvalues located near the origin of λ. The two largest eigenvalues may cross the axis $\mathrm{Re}(\lambda) = 0$, turning to complex unstable eigenvalues (Hopf bifurcation). Alternatively, the two eigenvalues may collide at $\mathrm{Im}(\lambda) = 0$

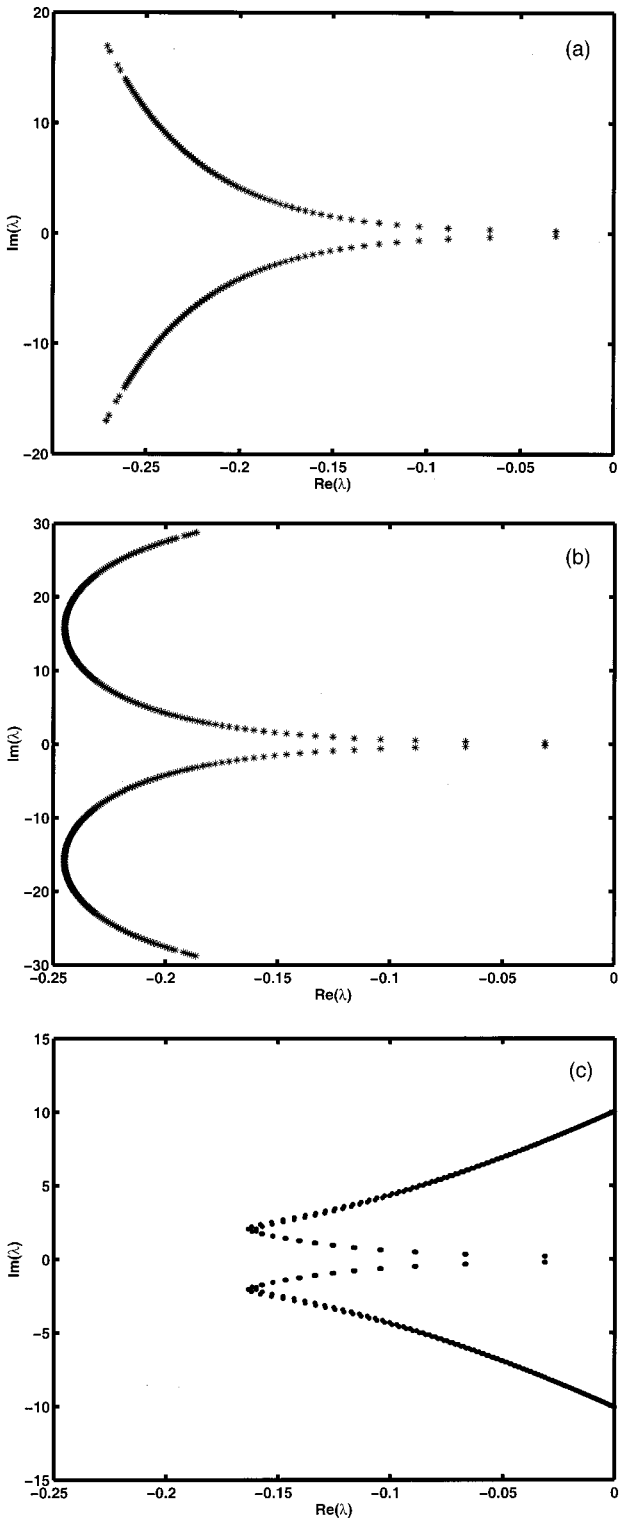

Fig. 6. Spectrum of eigenvalues for $I_{out} = 0$, $L = 20$, and $n_{0k} = -0.15$. (a) The eigenvalues are found from the analytical solution (30) and (31). (b) The eigenvalues are found from the analytical solution (32) and (33). (c) The eigenvalues are found numerically from the linear matrix problem (28).

and $\mathrm{Re}(\lambda) < 0$. Then, one of the two real eigenvalues may cross the axis $\mathrm{Im}(\lambda) = 0$, leading to a single real unstable eigenvalue (real bifurcation). In order to study these two bifurcations, we trace eigenvalues (usually, of limited number) with $\mathrm{Re}(\lambda) > 0$ and $|\mathrm{Im}(\lambda)| < 10$ [see Fig. 6(c)].

When the Kerr nonlinearity is compensated exactly across the photonic grating, i.e., $n_{nl} = 0$, the spectrum of Eqs. (25)–(26) was proven to be stable and located for $\mathrm{Re}(\lambda) < 0$.[1] We confirm this fact numerically within the matrix eigenvalue problem (28). The degeneracy between two branches of the spectrum in Fig. 6(c) is destroyed for $I_{out} > 0$, but the two branches stay in the left half-plane of λ for any $I_{out} < I_{lim}$.

For $n_{nl} \neq 0$, some eigenvalues may in principle emerge to the right half-plane of λ through the Hopf or real bifurcations. However, when the constraints (4) and (5) are satisfied, we do not find any unstable eigenvalues in the matrix problem (28). Thus the in-phase and weakly out-of-phase gratings in the all-optical limiting regime are uniformly stable in the domain I of Fig. 2, i.e., the two branches of the spectrum of λ remain within the left half-plane of λ for the whole range of the transmitted intensity I_{out}. The stable spectrum explains the simple dynamics of the photonic gratings shown in Fig. 3. A perturbation of the stationary regime disappears by means of radiation through the ends of the structure.

When the constraint (5) is violated, the nonlinear periodic structure is in the locally multistable limiting regime, as in domain II of Fig. 2. Such structures occur for the long devices with weak nonlinearity management and strong out-of-phase linear grating. In this case, we find some unstable real and complex eigenvalues of λ in the matrix problem (28). Figures 7(a) and 7(b) show unstable eigenvalues λ of the matrix problem (28) for the out-of-phase grating with $n_{nl} = 1$ and $n_{0k} = -0.1$, when the transmission curve $I_{out}(I_{in})$ is shown in Fig. 7(c). Although the curve displays the one-to-one dependence, the constraint (5) is violated for the given material parameters. Then, the stationary regime has few unstable eigenvalues that emerge from the largest eigenvalues of the two branches of the spectrum of λ. A single complex pair of unstable eigenvalues crosses the stability threshold at $I_{out} \approx 0.074$ (Hopf bifurcation), and it exists for intermediate intensities $0.074 < I_{out} < 0.131$ [see Fig. 7(b)]. At $I_{out} = 0.131$, the complex pair merges into a pair of positive and negative real eigenvalues at the origin $\lambda = 0$. The unstable (positive) real eigenvalue exists for large intensities $0.131 < I_{out} < I_{lim} \approx 0.156$ [see Fig. 7(a)]. Thus all stationary regimes, including the limiting regime, are unstable for $I_{out} > 0.074$, or, equivalently, for $I_{in} > 0.0743$ [see Fig. 7(c)].

More unstable eigenvalues show up when parameters of the out-of-phase photonic gratings violate strongly the constraint (5). Figures 8(a) and 8(b) show unstable real and complex eigenvalues λ of the matrix problem (28) for the out-of-phase grating with $n_{nl} = 1$ and $n_{0k} = -0.15$, when the transmission curve $I_{out}(I_{in})$ is shown in Fig. 8(c). The curve has negative-slope branches of local multistability at small and intermediate intensities. These negative-slope branches are associated with real unstable eigenvalues in the linear spectrum [see Fig. 8(a)] that occurs at $I_{out} \approx 0.002$ [at the point of vertical slope of $I_{out}(I_{in})$]. Two real eigenvalues exist for $0.002 < I_{out} < 0.018$ [see Fig. 8(a)]. The two real eigenvalues turn

into pairs of complex eigenvalues according to two different possibilities. The first real eigenvalue simply disappears at $I_{\text{out}} \approx 0.018$, and then a pair of unstable complex eigenvalues show up at $I_{\text{out}} \approx 0.023$ with a nonzero imaginary part [see Fig. 8(b)]. The other real eigenvalue splits into a pair of complex eigenvalues at $I_{\text{out}} = 0.025$; this bifurcation happens at the origin $\lambda = 0$ [see Fig. 8(b)]. The first complex eigenvalue exists for I_{out}

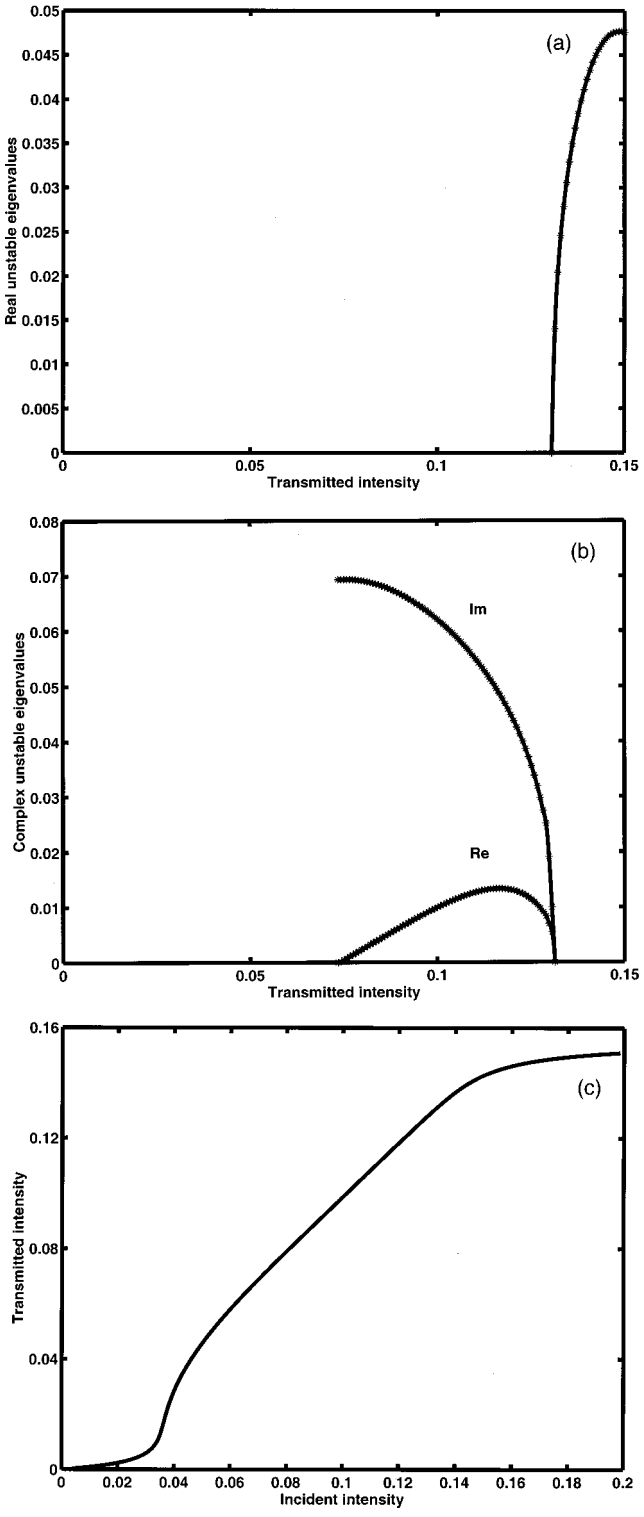

Fig. 7. Unstable (a) real and (b) complex eigenvalues versus the transmitted intensity I_{out} of the linear matrix problem (28) for the standardized photonic structure with material parameters $n_{\text{nl}} = 1$ and $n_{0\text{k}} = -0.1$. The input–output transmission characteristics $I_{\text{out}}(I_{\text{in}})$ is shown in (c).

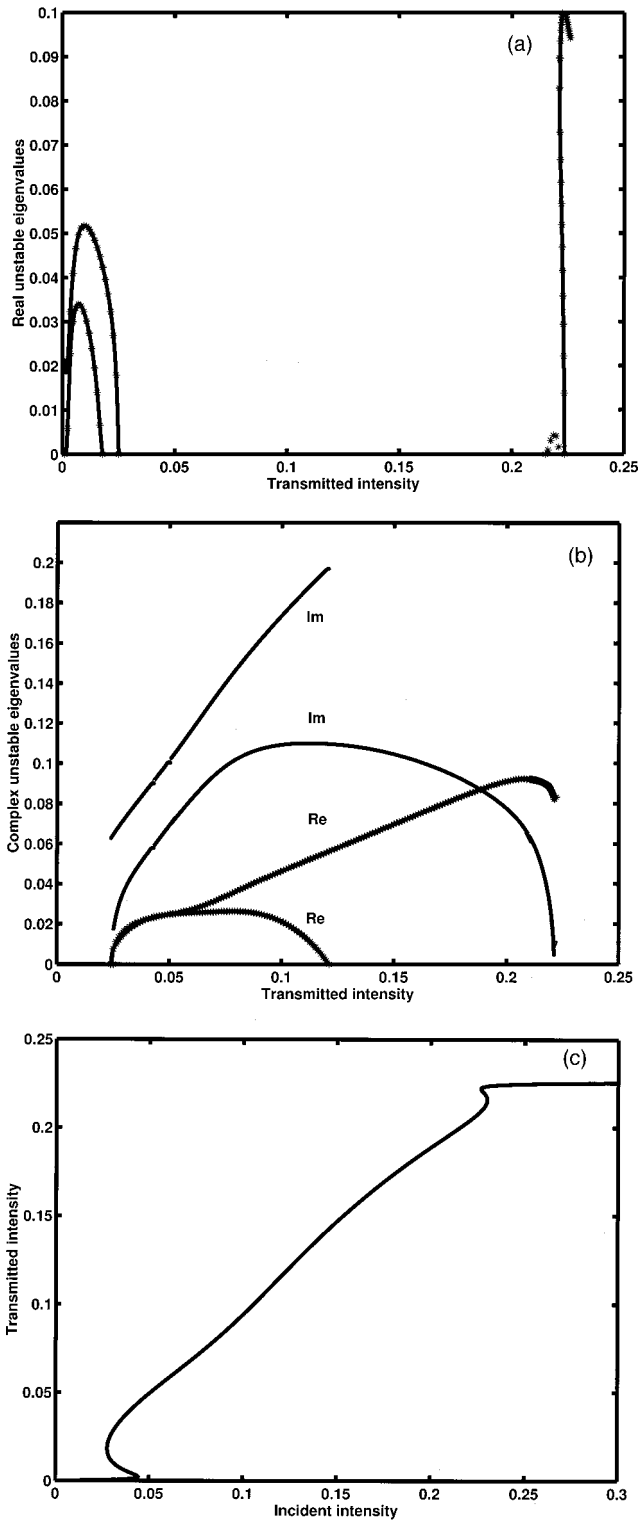

Fig. 8. Unstable (a) real and (b) complex eigenvalues versus the transmitted intensity I_{out} of the linear matrix problem (28) for the standardized photonic structure with material parameters $n_{\text{nl}} = 1$ and $n_{0\text{k}} = -0.15$. The input–output transmission characteristics $I_{\text{out}}(I_{\text{in}})$ is shown in (c), and it corresponds to curve II on Fig. 1.

< 0.121 and merges at $I_{out} \approx 0.121$ with the stable branches of λ. The other complex eigenvalue remains for the whole domain of existence of the stationary solution, and it switches back to a real eigenvalue at $I_{out} \approx 0.222$ (near the limiting value $I_{out} \approx I_{lim}$) [see Fig. 8(a)]. The latter bifurcation resembles the one shown in Figs. 7(a) and 7(b) for $n_{0k} = -0.1$.

Thus the stationary light transmission through the out-of-phase photonic grating with $n_{0k} = -0.15$ is unstable for $I_{out} > 0.002$, or, equivalently, for $I_{in} > 0.042$. The unstable spectrum explains the high-amplitude oscillations of the light transmission shown in Fig. 4. Indeed, the stationary regime of the photonic grating for $n_{nl} = 1$ and $n_{0k} = -0.15$ with $I_{out} = 0.12$ has a single pair of unstable complex eigenvalues [see Fig. 8(b)], and the imaginary part of the complex eigenvalue $\mathrm{Im}(\lambda) \approx 0.197$ matches well with a frequency of the high-amplitude oscillations in Fig. 4(c), $\Omega = 2\pi/T_{period} \approx 0.194$.

Strongly out-of-phase gratings have a complicated pattern of various instabilities. For instance, Figs. 9(a) and 9(b) display unstable eigenvalues of the matrix problem (28) for the out-of-phase grating with $n_{nl} = 1$ and $n_{0k} = -0.3$, and the curve $I_{out}(I_{in})$ is shown in Fig. 9(c). Even lower-transmissive states are instantaneously unstable with two real eigenvalues and a pair of complex eigenvalues [see Figs. 9(a) and 9(b)]. The unstable eigenvalues merge, disappear, and reappear in a number of bifurcations for larger values of I_{out}. However, there exist at least two unstable growth rates $\mathrm{Re}(\lambda) > 0$ for any value of the transmitted intensity I_{out}. Notice from Figs. 7, 8, and 9 that the growth rates become larger with larger negative values of n_{0k}.

When the constraint (4) is violated, the nonlinear periodic structure is in the multistability regime, as in domain III of Fig. 2. In this case, the stationary transmission regimes are widely unstable for both in-phase and out-of-phase photonic gratings. Figures 10(a) and 10(b) show a cascade of unstable eigenvalues for the multistable regime with $n_{nl} = 1.4$ and $n_{0k} = 0$, and the transmission curve $I_{out}(I_{in})$ is shown in Fig. 10(c). The first positive-slope branch of lower-transmissive states is stable for $I_{out} < 0.075$. The real unstable eigenvalue is clearly associated with the first negative-slope branch of transmissive states at $0.075 < I_{out} < 0.113$ [see Figs. 10(a) and 10(c)]. The two complex pairs of unstable eigenvalues are associated with the second positive-slope branch of higher-transmissive states that exists for $0.113 < I_{out} < 0.188$. However, the complex pairs emerge at $I_{out} \approx 0.139$, i.e., there is a stability window between $0.113 < I_{out} < 0.139$ for the highly transmissive states [see Figs. 10(b) and 10(c)]. These results recover conclusions of Ref. 8 obtained for the coupled-mode system (1)–(2) with $n_{2k} = 0$.

Starting with $I_{out} > 0.139$, all positive-slope branches of higher-transmissive states are unstable since the complex eigenvalues do not disappear for larger values of I_{out} [see Fig. 10(b)]. Moreover, the number of complex eigenvalues grows with each positive-slope branch, e.g., two more complex pairs emerge for the third positive-slope branch of higher-transmissive states at $I_{out} > 0.250$ [see Figs. 10(b) and 10(c)]. The real unstable eigenvalues match all negative-slope branches of transmissive states and also some higher-order positive-slope states as well [see Figs. 10(a) and 10(c)]. Thus we conclude that the stationary states in the multistable regime are unstable except for the first positive-slope branch of lower-

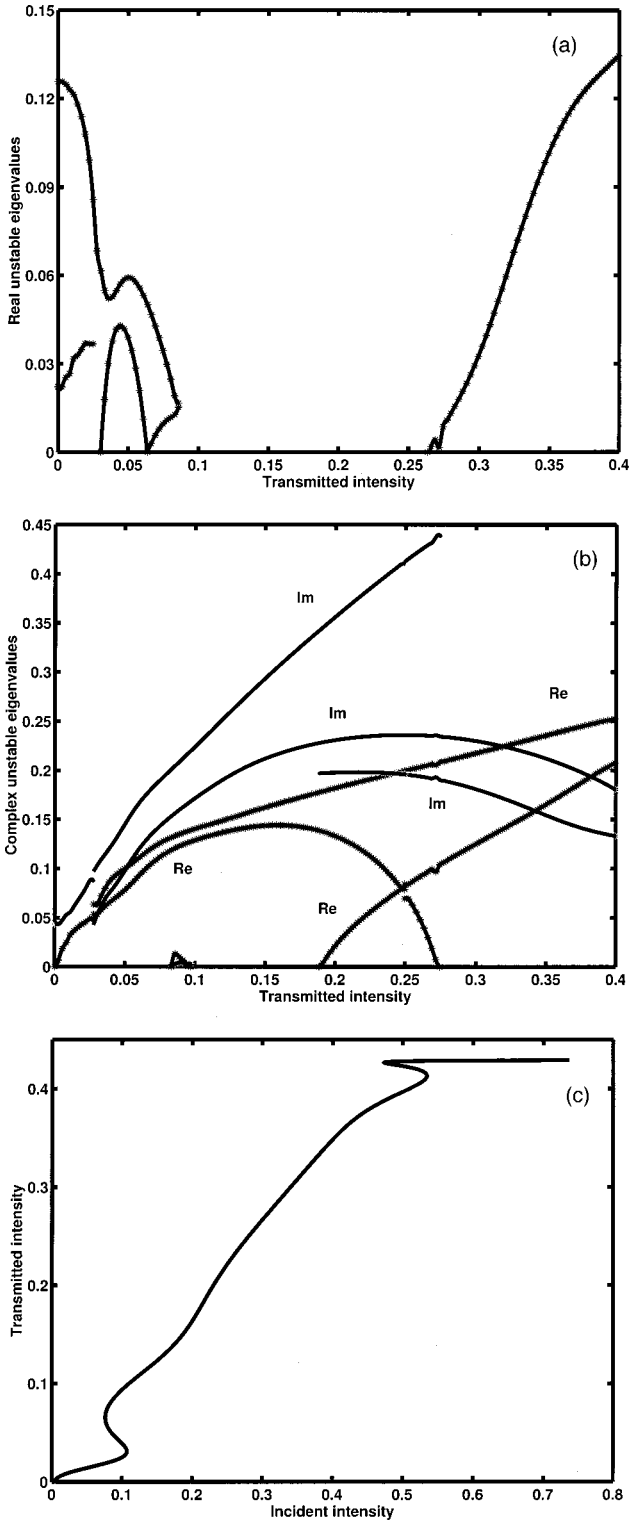

Fig. 9. Unstable (a) real and (b) complex eigenvalues versus the transmitted intensity I_{out} of the linear matrix problem (28) for the standardized photonic structure with material parameters $n_{nl} = 1$ and $n_{0k} = -0.3$. The input–output transmission characteristics $I_{out}(I_{in})$ is shown in (c).

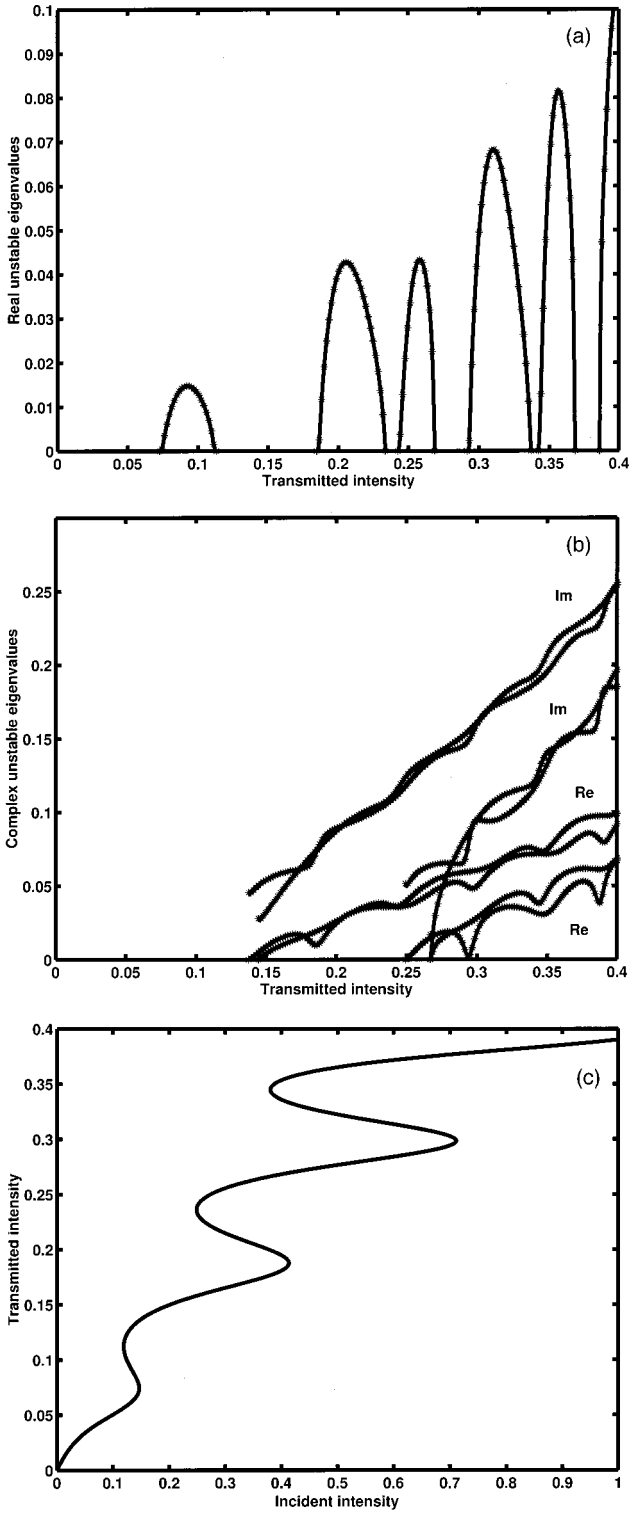

Fig. 10. Unstable (a) real and (b) complex eigenvalues versus the transmitted intensity I_{out} of the linear matrix problem (28) for the standardized photonic structure with material parameters $n_{\text{nl}} = 1.4$ and $n_{0\text{k}} = 0$. The input–output transmission characteristics $I_{\text{out}}(I_{\text{in}})$ is shown in (c), and it corresponds to curve III in Fig. 1.

transmissive states and except for a narrow window for the second positive-slope branch of higher-transmissive states. In particular, these results explain the switching dynamics of the photonic gratings shown in Figs. 5(a) and 5(b). The stationary regime with $I_{\text{out}} = 0.090$ has a single unstable real eigenvalue [see Fig. 10(a)], and this instability exhibits a switching of the light transmission to the stable fundamental state with a smaller value of the transmitted intensity $I_{\text{out}} = 0.062$ [see Fig. 5(a)].

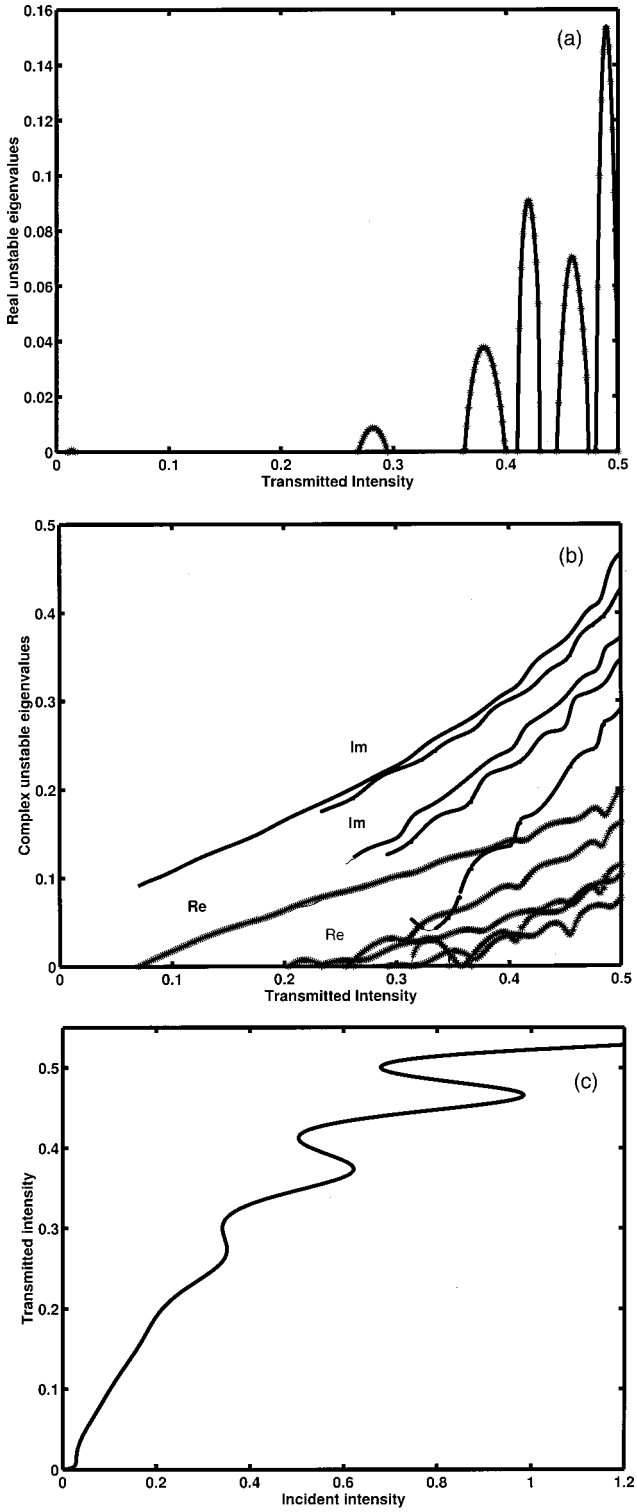

Fig. 11. Unstable (a) real and (b) complex eigenvalues versus the transmitted intensity I_{out} of the linear matrix problem (28) for the standardized photonic structure with material parameters $n_{\text{nl}} = 1.4$ and $n_{0\text{k}} = -0.1$. The input–output transmission characteristics $I_{\text{out}}(I_{\text{in}})$ is shown in (c).

A linear grating added to the nonlinear periodic structure, when $n_{0k} \neq 0$, may change stability results described above. Figures 11(a) and 11(b) show the unstable eigenvalues for the out-of-phase grating with $n_{nl} = 1.4$ and $n_{0k} = -0.1$, when the transmission curve $I_{out}(I_{in})$ is shown in Fig. 11(c). The transmission curve has the first positive-slope branch of lower-transmissive states extended up to higher intensities $I_{out} < 0.272$. However, these positive-slope states are still unstable for $0.083 < I_{out} < 0.272$ due to a single pair of complex eigenvalues [see Fig. 11(b)]. The rest of the picture in Figs. 11(a) and 11(b) resembles the case $n_{0k} = 0$ in Figs. 10(a) and 10(b). The pattern features real unstable eigenvalues in narrow intervals of I_{out} and pairs of complex unstable eigenvalues in semi-infinite intervals of I_{out}. Thus the out-of-phase linear grating does not improve stability of lower-transmissive states because of oscillatory instabilities.

We conclude that the all-optical limiting regime is linearly stable for in-phase and weakly out-of-phase gratings. Moderate out-of-phase linear gratings are destabilized through complex (Hopf) bifurcations. Strong out-of-phase gratings are widely unstable because of local multistability at small incident intensities. The transition from the limiting regime to multistability results in loss of stability for both in-phase and out-of-phase gratings except for the first positive-slope branch of lower-transmissive states. However, the first positive-slope branch is also unstable for strong out-of-phase gratings due to oscillatory bifurcations.

6. DYNAMICS OF LIGHT TRANSMISSION IN THE PERIODIC STRUCTURE

Here we model the time-dependent response of the nonlinear periodic structure under the incident light wave. We show that the time-dependent response of the photonic device can be predicted by the number and type of unstable eigenvalues in the spectrum of the linear stability problem. The incident light is modeled by the coupled-mode equations (1)–(2) with the varying boundary condition (6):

$$I_{in}(t) = I_0 \tanh t, \quad \theta_{in}(t) = 0. \tag{34}$$

The incident light represents a continuous wave of varying amplitude that switches monotonically from zero intensity to a constant intensity I_0. The transition happens during the time interval $(\Delta t) \approx 1$ in the layer near the left end of the structure $(\Delta z) \approx 1 \ll L = 20$. We assume that light waves are initially zero throughout the structure, i.e., $A_{\pm}(z, 0) = 0$.

If the stationary regime with a constant incident light intensity $I_{in} = I_0$ is linearly stable, we expect that illuminating light at the input end of the structure leads to formation of the stationary-transmission regime inside the structure. The transition to the stable-stationary regime is illustrated in Fig. 12 for the photonic grating with $n_{nl} = 1$ and $n_{0k} = 0$. The photonic structure is in the all-optical limiting regime, i.e., in the domain I of Fig. 2. The stability analysis shows no unstable eigenvalues of the linearized problem. The transmitted intensities are limited by the value $I_{out} < I_{lim} \approx 0.049$.

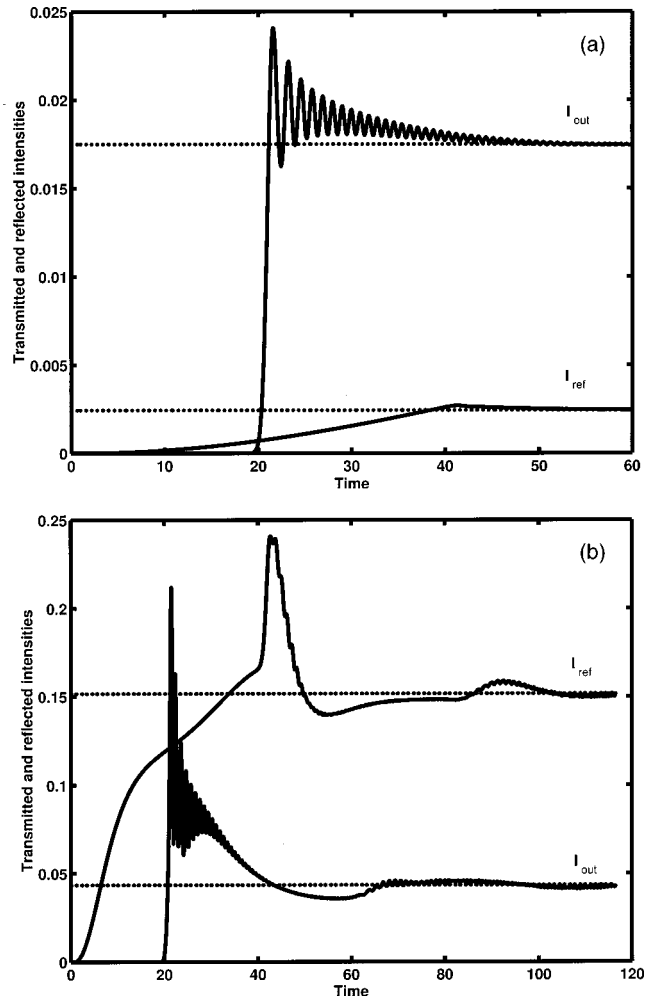

Fig. 12. Transmitted $[I_{out}(t)]$ and reflected $[I_{ref}(t)]$ intensities as functions of time t. The incident intensity $I_{in}(t)$ is given by Eqs. (34) for (a) $I_0 = 0.02$ and (b) $I_0 = 0.2$. The standardized photonic structure has the material parameters $n_{nl} = 1$ and $n_{0k} = 0$. The dotted curves display constant values of I_{out} and I_{ref} for stationary transmission that correspond to the incident intensity $I_{in} = I_0$.

The numerical simulations with the varying boundary condition (34) for $I_0 = 0.020$ show fast relaxation of the light waves to the stable stationary regime with $I_{in} = 0.020$ and $I_{out} = 0.018$ [see Fig. 12(a)]. The two curves display transmitted $[I_{out}(t)]$ and reflected $[I_{ref}(t)]$ intensities as functions of time t. The constant levels for I_{out} and I_{ref} in the stationary-transmission regime with the same value of $I_{in} = I_0$ are plotted by dotted curves. The incident wave is highly transmissive in the stationary regime, i.e., the reflected wave is small.

When the light intensity is increased, e.g., for $I_0 = 0.2$, the same relaxation to the stable stationary regime becomes slowly convergent. The dynamics of light waves is accompanied by a large-amplitude transient wave front and with few additional oscillations [see Fig. 12(b)]. The stationary transmission occurs for $I_{in} = 0.2$ and $I_{out} = 0.043$. In this case, the reflected-wave intensity I_{ref} is larger than the transmitted-wave intensity I_{out}, i.e., the stationary state is lower transmissive.

The transient oscillations in Fig. 12(b) can be explained by the largest eigenvalues of the linearized problem, which have the smallest negative real part and a nonzero imaginary part. Such eigenvalues do not cross the stability threshold for the stable structure with $n_{\rm nl} = 1$ and $n_{0\rm k} = 0$. However, they are still close to the threshold $\mathrm{Re}(\lambda) = 0$, and the negative real part of the largest eigenvalues becomes smaller with larger values of I_0. As a result, the incident waves of large intensities I_0 converge to the near-limiting stationary regime very slowly, with sufficiently large computational errors.

If the stationary regime becomes unstable, we expect that the transition induced by the incident wave (34) results in the nonstationary dynamics. The dynamics depends on the dominant unstable eigenvalues of the linear stability problem. The out-of-phase photonic structure with $n_{\rm nl} = 1$ and $n_{0\rm k} = -0.15$ is in the locally multistable limiting regime, i.e., in domain II of Fig. 2. The transmitted intensities are limited by the value $I_{\rm out} < I_{\rm lim} \approx 0.227$. The stationary regimes have real unstable eigenvalues for $0.002 < I_{\rm out} < 0.018$ and complex eigenvalues for $0.018 < I_{\rm out} < 0.222$ [see Figs. 8(a) and 8(b)]. Therefore only the lower branch of lower-transmissive states is stable, and the incident waves are unstable for all intensities: $I_{\rm in} > 0.042$. The dynamics of unstable transitions is shown in Figs. 13(a) and 13(b) for the values $I_0 = 0.030$ (a) and $I_0 = 0.075$ (b).

There are three stationary regimes corresponding to the incident intensity $I_0 = 0.030$ [see Fig. 8(c)]. The intermediate branch is unstable with two real unstable eigenvalues [see Fig. 8(a)], and the upper branch is unstable with two complex pairs of eigenvalues [see Fig. 8(b)]. As a result, the incident wave selects the lower stable branch of stationary transmission. The stable branch has extremely small transmitted intensity $I_{\rm out} \approx 0.00057$ [see Fig. 13(a)], i.e., the incident wave is highly reflected for $I_0 = 0.030$. Notice from Fig. 13(a) that the convergence to the stable stationary regime is oscillatory. The oscillatory convergence indicates the presence of complex eigenvalues λ in the linearized problem with a small but negative real part. These eigenvalues destabilize the photonic structure with larger intensities I_0 of the incident light.

For larger values of incident intensities, e.g., for $I_0 = 0.075$, no stable lower-transmissive state exists, and the higher-transmissive state with $I_{\rm in} = 0.075$ and $I_{\rm out} = 0.07$ is unstable with two complex pairs of unstable eigenvalues. As a result, the incident wave generates nonstationary transmission accompanied by two-frequency synchronized oscillations [see Fig. 13(b)]. Notice that for yet larger values of I_0, one complex pair of unstable eigenvalues disappear, and the instability has a single frequency [see Fig. 8(b)]. Then, the response of the photonic structure to the incident light becomes a one-frequency high-amplitude oscillation, similar to Fig. 4(c) obtained for the same structure under the incident light with $I_{\rm in} = 0.124$ and $I_{\rm out} = 0.12$.

Similar nonstationary dynamics is observed for the multistable photonic structures in domain III of Fig. 2. For example, we consider the multistable structure with $n_{\rm nl} = 1.4$ and $n_{0\rm k} = 0$. The stationary regimes are all

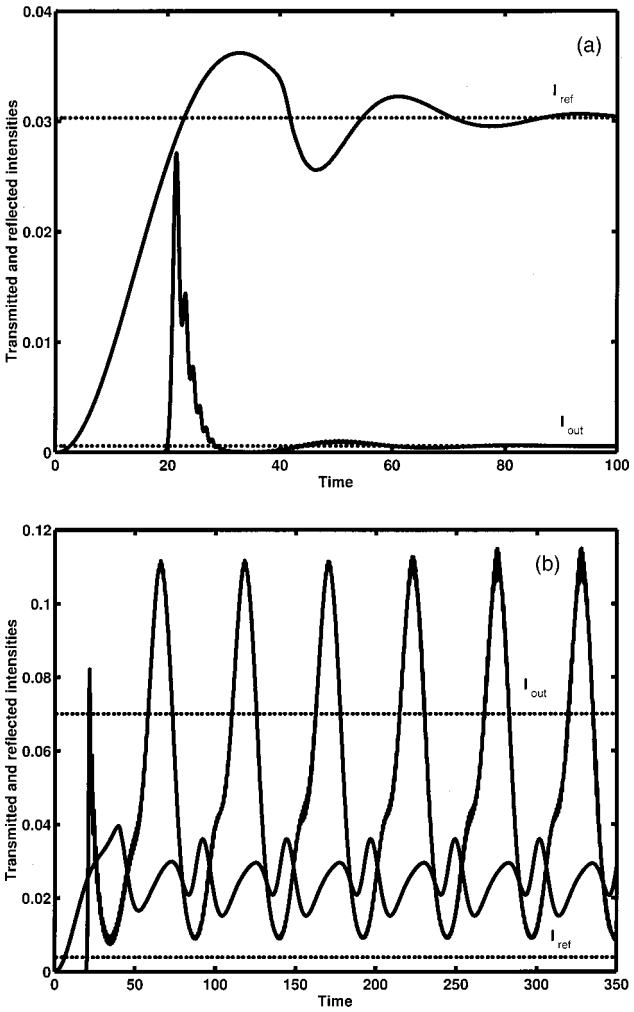

Fig. 13. Transmitted $[I_{\rm out}(t)]$ and reflected $[I_{\rm ref}(t)]$ intensities as functions of time t. The incident intensity $I_{\rm in}(t)$ is given by Eqs. (34) for (a) $I_0 = 0.030$ and (b) $I_0 = 0.075$. The standardized photonic structure has the material parameters $n_{\rm nl} = 1$ and $n_{0\rm k} = -0.15$. The dotted curves display constant values of stationary intensities $I_{\rm out}$ and $I_{\rm ref}$, respectively, that correspond to the incident intensity $I_{\rm in} = I_0$.

unstable for incident intensities $I_{\rm in} > 0.152$, when the incident intensity exceeds the maximal intensity of the lowest branch in Fig. 10(c).

The dynamics of unstable transitions is shown in Fig. 14 for $I_0 = 0.2$. The stationary-transmission regime with $I_{\rm in} = 0.2$ and $I_{\rm out} = 0.148$ has two pairs of complex unstable eigenvalues [see Fig. 10(b)]. As a result, the transition dynamics results in high-amplitude oscillations around the unstable stationary-transmission regime [see Fig. 14(a)]. The oscillations are observed for longer times with no visible distortions both for transmitted and reflected intensities. These oscillations correspond to the regime of periodic generation of Bragg solitons discussed in Ref. 11. The Bragg solitons are periodically generated at the left end of the structure and transmitted to the right end of the structure, resulting in high-amplitude oscillations in Fig. 14(a). The snapshot of the forward and backward waves is shown in Figs. 14(b) and 14(c). A single Bragg soliton is clearly seen to move across the photonic device.

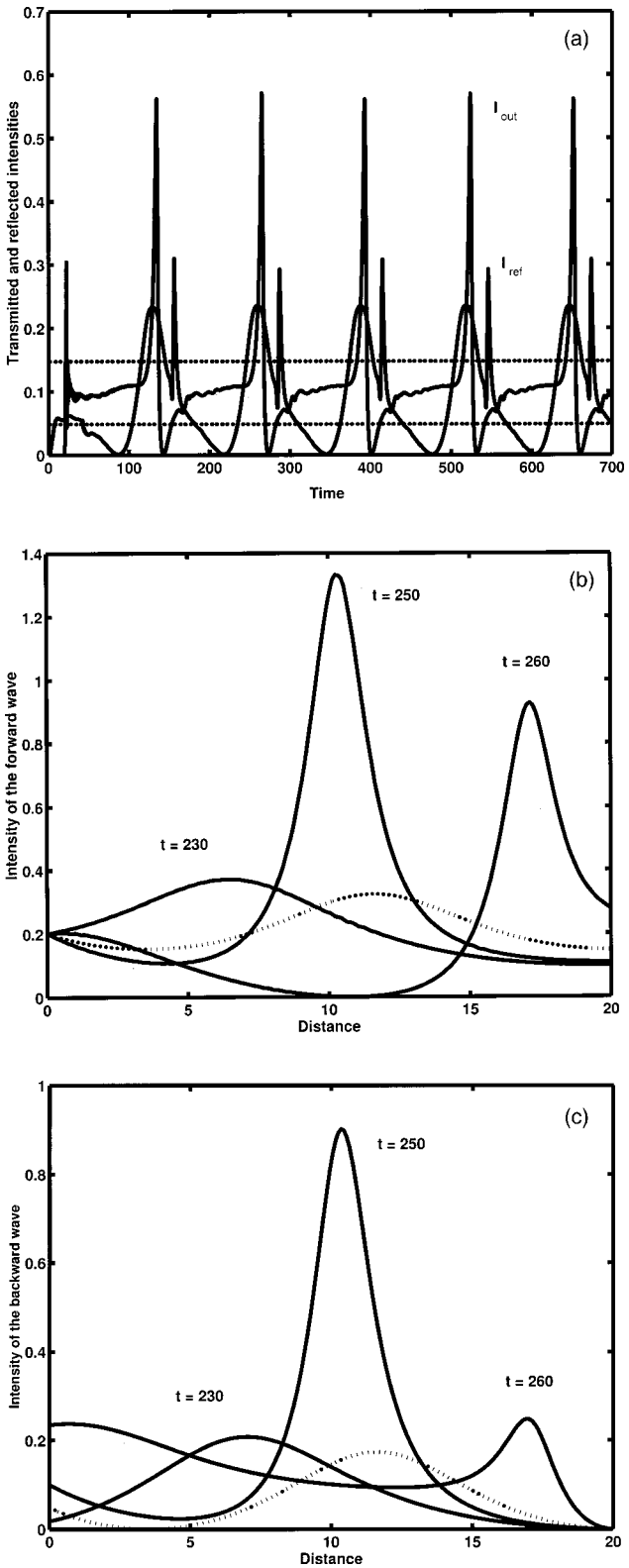

Fig. 14. (a) Transmitted $[I_{\text{out}}(t)]$ and reflected $[I_{\text{ref}}(t)]$ intensities as functions of time t. (b),(c) The intensities of the forward wave $|A_+|^2$ and the backward wave $|A_-|^2$ across the photonic device at the time instances $t = 230$, $t = 250$, and $t = 260$. The incident intensity $I_{\text{in}}(t)$ is given by Eqs. (34) for $I_0 = 0.2$. The standardized photonic structure has the material parameters $n_{\text{nl}} = 1.4$ and $n_{0\text{k}} = 0$. The dotted curves display stationary intensities and distributions that correspond to the incident intensity $I_{\text{in}} = 0.2$.

For larger incident intensities I_0, the stationary transmission becomes highly unstable with more pairs of complex eigenvalues [see Fig. 10(b)]. The numerical observations show the blowup of the light wave intensities that occurs in the middle of the photonic structure in a finite time. The blowup profile resembles the Bragg solitons in Figs. 14(b) and 14(c), but the light intensity of the soliton grows with no limits, eventually burning the photonic structure. We do not pursue the blowup phenomenon in this paper, since such large intensities are highly unlikely to be used in realistic photonic devices.

We conclude that real and complex unstable eigenvalues of the linear stability problem do predict accurately long-term dynamics of the periodic nonlinear structure illuminated by the incident light. When all eigenvalues are located in the left half-plane of λ, the light transmission relaxes to a stable stationary regime. When unstable eigenvalues emerge into the right half-plane of λ as real eigenvalues, the light transmission switches from a highly transmissive unstable state to the stable lower-transmissive state, if it exists. When the lower branch does not exist, the unstable eigenvalues are complex valued, and the light transmission results in nonstationary dynamics with high-amplitude oscillations and periodic generation of Bragg solitons. This conclusion generalizes the results of Ref. 11 obtained for the case $n_{2\text{k}} = 0$.

Thus the photonic devices have unstable stationary transmissions in the domains II and III. In particular, the out-of-phase linear gratings become unstable for $n_{\text{nl}} \neq 0$. Although the out-of-phase gratings feature the two-step linear map in the input–output transmission curve that is useful for many applications, such as logic functions and signal processing, the light transmission in the out-of-phase gratings displays complicated nonstationary dynamics, unless the Kerr nonlinearities are carefully managed with zero net-average nonlinearity. In reality, the nonlinearities are affected by temperature fluctuations, and it is thus very hard to maintain the stable all-optical limiting regime for the photonic devices.

APPENDIX A: NUMERICAL METHOD FOR THE TIME-EVOLUTION SYSTEM (8)–(9)

We start with the system (8)–(9) and replace the derivative by central differences according to the Crank–Nicholson method for the wave equation (16). Then we arrive at the system of difference equations

$$u_{n,k+1} + r(u_{n+1,k+1} - u_{n-1,k+1}) + \kappa y_{n,k+1} = u_{n,k-1} - r(u_{n+1,k-1} - u_{n-1,k-1}) - \kappa y_{n,k-1} - F_{un,k}, \tag{A1}$$

$$w_{n,k+1} + r(w_{n+1,k+1} - w_{n-1,k+1}) - \kappa v_{n,k+1} = w_{n,k-1} - r(w_{n+1,k-1} - w_{n-1,k-1}) + \kappa v_{n,k-1} + F_{wn,k}, \tag{A2}$$

$$v_{n,k+1} - r(v_{n+1,k+1} - v_{n-1,k+1}) + \kappa w_{n,k+1} = v_{n,k-1} + r(v_{n+1,k-1} - v_{n-1,k-1}) - \kappa w_{n,k-1} - F_{vn,k}, \tag{A3}$$

$$y_{n,k+1} - r(y_{n+1,k+1} - y_{n-1,k+1}) - \kappa u_{n,k+1} = y_{n,k-1} + r(y_{n+1,k-1} - y_{n-1,k-1}) + \kappa u_{n,k-1} + F_{yn,k}, \tag{A4}$$

where

$$r = \frac{\tau}{2h}, \quad \kappa = \tau n_{0k},$$

and the nonlinear vectors are computed from the nonlinear functions (10), e.g.,

$$F_{un,k} = 2\tau f_u(u_{n,k}, w_{n,k}, v_{n,k}, y_{n,k}).$$

The system (A1)–(A4) is set at the interior grid points, when $n = 1,2,\ldots,N$. The boundary values $u_{N+1,k}$, $w_{N+1,k}$, $v_{0,k}$, and $y_{0,k}$ are also unknowns in the vectors (14), and they should be considered separately. The three-point forward (for v and y at $z = 0$) and backward (for u and w at $z = L$) differences have the same local truncation error as the central differences used in Eqs. (A1)–(A4). Using the three-point differences for approximations of space derivatives in the system (8)–(9) for $z = 0$ and $z = L$, we complete the system of difference equations (A1)–(A4) by four end-point equations:

$$u_{N+1,k+1} + r(3u_{N+1,k+1} - 4u_{N,k+1} + u_{N-1,k+1}) = u_{N+1,k-1} - r(3u_{N+1,k-1} - 4u_{N,k-1} + u_{N-1,k-1}) - F_{uN+1,k}, \tag{A5}$$

$$w_{N+1,k+1} + r(3w_{N+1,k+1} - 4w_{N,k+1} + w_{N-1,k+1}) = w_{N+1,k-1} - r(3w_{N+1,k-1} - 4w_{N,k-1} + w_{N-1,k-1}) + F_{wN+1,k}, \tag{A6}$$

$$v_{0,k+1} - r(-v_{2,k+1} + 4v_{1,k+1} - 3v_{0,k+1}) = v_{0,k-1} + r(-v_{2,k-1} + 4v_{1,k-1} - 3v_{0,k-1}) - \kappa(w_{0,k+1} + w_{0,k-1}) - F_{v0,k}, \tag{A7}$$

$$y_{0,k+1} - r(-y_{2,k+1} + 4y_{1,k+1} - 3y_{0,k+1}) = y_{0,k-1} + r(-y_{2,k-1} + 4y_{1,k-1} - 3y_{0,k-1}) + \kappa(u_{0,k+1} + u_{0,k-1}) + F_{y0,k}, \tag{A8}$$

where the boundary conditions (15) compliment the system (A7)–(A8). The coupled system (A1)–(A8) can be transformed to the matrix form (17)–(18) with the coefficient matrices

$$A(r) = \begin{bmatrix} 1 & r & 0 & \cdots & 0 & 0 & 0 \\ -r & 1 & r & \cdots & 0 & 0 & 0 \\ 0 & -r & 1 & \cdots & 0 & 0 & 0 \\ \vdots & \vdots & \vdots & \ddots & \vdots & \vdots & \vdots \\ 0 & 0 & 0 & \cdots & -r & 1 & r \\ 0 & 0 & 0 & \cdots & r & -4r & 1+3r \end{bmatrix}, \tag{A9}$$

$$B(r) = \begin{bmatrix} 1+3r & -4r & r & \cdots & 0 & 0 & 0 \\ r & 1 & -r & \cdots & 0 & 0 & 0 \\ 0 & r & 1 & \cdots & 0 & 0 & 0 \\ \vdots & \vdots & \vdots & \ddots & \vdots & \vdots & \vdots \\ 0 & 0 & 0 & \cdots & r & 1 & -r \\ 0 & 0 & 0 & \cdots & 0 & r & 1 \end{bmatrix}, \tag{A10}$$

$$I_+ = \begin{bmatrix} 0 & 1 & 0 & \cdots & 0 & 0 & 0 \\ 0 & 0 & 1 & \cdots & 0 & 0 & 0 \\ \vdots & \vdots & \vdots & \ddots & \vdots & \vdots & \vdots \\ 0 & 0 & 0 & \cdots & 0 & 0 & 1 \\ 0 & 0 & 0 & \cdots & 0 & 0 & 0 \end{bmatrix},$$

$$I_- = \begin{bmatrix} 0 & 0 & 0 & \cdots & 0 & 0 & 0 \\ 1 & 0 & 0 & \cdots & 0 & 0 & 0 \\ \vdots & \vdots & \vdots & \ddots & \vdots & \vdots & \vdots \\ 0 & 0 & 0 & \cdots & 1 & 0 & 0 \\ 0 & 0 & 0 & \cdots & 0 & 1 & 0 \end{bmatrix}. \tag{A11}$$

The right-hand side vectors in Eqs. (17)–(18) are computed as

$$\mathbf{H}_{uk} = r(u_{0,k+1} + u_{0,k-1})\mathbf{e}_1 - \mathbf{F}_{uk}, \tag{A12}$$

$$\mathbf{H}_{wk} = r(w_{0,k+1} + w_{0,k-1})\mathbf{e}_1 + \mathbf{F}_{wk}, \tag{A13}$$

$$\mathbf{H}_{vk} = -\kappa(w_{0,k+1} + w_{0,k-1})\mathbf{e}_1 - \mathbf{F}_{vk}, \tag{A14}$$

$$\mathbf{H}_{yk} = \kappa(u_{0,k+1} + u_{0,k-1})\mathbf{e}_1 + \mathbf{F}_{yk}, \tag{A15}$$

where $\mathbf{e}_1$ is the first unit vector in $\mathcal{R}^{N+1}$ and $\mathbf{F}_{uk}$, $\mathbf{F}_{wk}$, $\mathbf{F}_{vk}$, and $\mathbf{F}_{yk}$ are right-hand-side vectors in $\mathcal{R}^{N+1}$ constructed from values of $F_{un,k}$, $F_{wn,k}$, $F_{vn,k}$, and $F_{yn,k}$ similarly to the vectors $\mathbf{u}_k$, $\mathbf{w}_k$, $\mathbf{v}_k$, and $\mathbf{y}_k$ in Eqs. (14).

APPENDIX B: NUMERICAL METHOD FOR THE EIGENVALUE PROBLEM (25)–(26)

The central-difference equations for the system (25)–(26) have the form

$$-(u_{n+1} - u_{n-1}) - \kappa y_n - F'_{un} = \gamma u_n, \tag{B1}$$

$$-(w_{n+1} - w_{n-1}) + \kappa v_n + F'_{wn} = \gamma w_n, \tag{B2}$$

$$(v_{n+1} - v_{n-1}) - \kappa w_n - F'_{vn} = \gamma v_n, \tag{B3}$$

$$(y_{n+1} - y_{n-1}) + \kappa u_n + F'_{yn} = \gamma y_n, \tag{B4}$$

where

$$\kappa = 2hn_{0k}, \quad \gamma = 2h\lambda,$$

and the nonlinear vectors are computed from the nonlinear functions (27), e.g.,

$$F'_{un} = 2hf'_u(u_{0n}, w_{0n}, v_{0n}, y_{0n}; u_n, w_n, v_n, y_n).$$

In the system (B1)–(B4), we have dropped the subindex of the functions u_1, w_1, v_1, and y_1 compared with the system (25)–(26). The system (B1)–(B4) should be complimented by four additional equations for boundary elements. We use again the three-point forward difference for v and y at $z = 0$ and the three-point backward difference for u and w at $z = L$. Then, the end-point equations are derived as

$$-(3u_{N+1} - 4u_N + u_{N-1}) - F'_{uN+1} = \gamma u_{N+1}, \quad \text{(B5)}$$

$$-(3w_{N+1} - 4w_N + w_{N-1}) + F'_{wN+1} = \gamma w_{N+1}, \quad \text{(B6)}$$

$$(-3v_0 + 4v_1 - v_2) - F'_{v0} = \gamma v_0, \quad \text{(B7)}$$

$$(-3y_0 + 4y_1 - y_2) + F'_{y0} = \gamma y_0, \quad \text{(B8)}$$

where we have used the zero boundary conditions (24) for u_0, w_0, v_{N+1}, and y_{N+1}. The coupled system (B1)–(B8) can be transformed to the matrix form (28) with the coefficient matrices

$$A_\infty = \begin{bmatrix} 0 & -1 & 0 & . & . & . & 0 & 0 & 0 \\ 1 & 0 & -1 & . & . & . & 0 & 0 & 0 \\ 0 & 1 & 0 & . & . & . & 0 & 0 & 0 \\ . & . & . & . & . & . & . & . & . \\ 0 & 0 & 0 & . & . & . & 1 & 0 & -1 \\ 0 & 0 & 0 & . & . & . & -1 & 4 & -3 \end{bmatrix}, \quad \text{(B9)}$$

$$B_\infty = \begin{bmatrix} -3 & 4 & -1 & . & . & . & 0 & 0 & 0 \\ -1 & 0 & 1 & . & . & . & 0 & 0 & 0 \\ 0 & -1 & 0 & . & . & . & 0 & 0 & 0 \\ . & . & . & . & . & . & . & . & . \\ 0 & 0 & 0 & . & . & . & -1 & 0 & 1 \\ 0 & 0 & 0 & . & . & . & 0 & -1 & 0 \end{bmatrix}. \quad \text{(B10)}$$

In the system (28), the coefficient matrices $I_\pm$ are defined in Eqs. (A11) of Appendix A, and the matrix $\mathcal{U}$ is computed as

$$\mathcal{U} = \begin{bmatrix} -\mathbf{F}'_u \\ \mathbf{F}'_y \\ \mathbf{F}'_w \\ -\mathbf{F}'_v \end{bmatrix}, \quad \text{(B11)}$$

where $\mathbf{F}'_u$, $\mathbf{F}'_w$, $\mathbf{F}'_v$, and $\mathbf{F}'_y$ are now $(N+1) \times 4(N+1)$ matrices that are computed from values of $\mathbf{F}'_{un}$, $\mathbf{F}'_{wn}$, $\mathbf{F}'_{vn}$, and $\mathbf{F}'_{yn}$.

REFERENCES

1. D. Pelinovsky, J. Sears, L. Brzozowski, and E. H. Sargent, "Stable all-optical limiting in nonlinear periodic structures. I. Analysis," J. Opt. Soc. Am. B **19**, 43–53 (2002).
2. L. Brzozowski and E. H. Sargent, "Nonlinear distributed feedback structures as passive optical limiters," J. Opt. Soc. Am. B **17**, 1360–1365 (2000).
3. C. M. de Sterke and J. E. Sipe, "Gap solitons," Prog. Opt. **33**, 203–260 (1994).
4. H. G. Winful, J. H. Marburger, and E. Garmire, "Theory of bistability in nonlinear distributed feedback structure," Appl. Phys. Lett. **35**, 379–381 (1979).
5. H. M. Gibbs, *Optical Bistability: Controlling Light with Light* (Academic, New York, 1985).
6. W. Chen and D. L. Mills, "Optical response of nonlinear multilayer structures: bilayers and superlattices," Phys. Rev. B **36**, 6269–6278 (1987).
7. J. He and M. Cada, "Optical bistability in semiconductor periodic structures," IEEE J. Quantum Electron. **27**, 1182–1188 (1991).
8. C. M. de Sterke, "Stability analysis of nonlinear periodic media," Phys. Rev. A **45**, 8252–8258 (1992).
9. Yu. N. Ovchinnikov, "Stability problem in nonlinear wave propagation," JETP **87**, 807–813 (1998).
10. H. G. Winful and G. D. Cooperman, "Self-pulsing and chaos in distributed feedback bistable optical devices," Appl. Phys. Lett. **40**, 298–300 (1982).
11. C. M. de Sterke and J. E. Sipe, "Switching dynamics of finite periodic nonlinear media: a numerical study," Phys. Rev. A **42**, 2858–2869 (1990).
12. G. P. Agrawal, *Nonlinear Fiber Optic* (Academic, San Diego, 1989), Chap. 7.
13. C. M. de Sterke, K. R. Jackson, and B. D. Robert, "Nonlinear coupled-mode equations on a finite interval: a numerical procedure," J. Opt. Soc. Am. B **8**, 403–412 (1991).